Naval Research Laboratory

Washington, DC 20375-5320

NRL/MR/6930--18-9819

Colorimetric Biosensor: Porphyrin Variations

Brandy J. White

Laboratory for the Study of Molecular Interfacial Interactions
Center for Bio/Molecular Science & Engineering

Chris R. Taitt

Laboratory for Biomolecular Dynamics
Center for Bio/Molecular Science & Engineering

Apre Gleaves

Chemistry Department, Howard University
Washington, DC

Edikan Archibong

Department of Chemical and Biomedical Engineering, University of South Florida
Tampa, FL

Stormie Monk

Fayetteville State University
Fayetteville, NC

Iwona A. Leska

Nova Research, Inc.
Alexandria, VA

October 3, 2018

REPORT DOCUMENTATION PAGE

Form Approved
OMB No. 0704-0188

1. REPORT DATE *(DD-MM-YYYY)*	**2. REPORT TYPE**	**3. DATES COVERED** *(From - To)*
03-10-2018	Memorandum Report	0/01/2012 - 08/01/2018

4. TITLE AND SUBTITLE

Colorimetric Biosensor: Porphyrin Variations

5a. CONTRACT NUMBER

5b. GRANT NUMBER

5c. PROGRAM ELEMENT NUMBER

6. AUTHOR(S)

Brandy J. White, Chris R. Taitt, Apre Gleaves*, Edikan Archibong**, Stormie Monk+ and Iwona Leska++

5d. PROJECT NUMBER

5e. TASK NUMBER

5f. WORK UNIT NUMBER
69-6A26

7. PERFORMING ORGANIZATION NAME(S) AND ADDRESS(ES)

Center for Bio/Molecular Science & Engineering
Naval Research Laboratory
4555 Overlook Avenue, SW
Washington, DC 20375-5344

8. PERFORMING ORGANIZATION REPORT NUMBER

NRL/MR/6930--18-9819

9. SPONSORING / MONITORING AGENCY NAME(S) AND ADDRESS(ES)

10. SPONSOR / MONITOR'S ACRONYM(S)
NRL 6.2

11. SPONSOR / MONITOR'S REPORT NUMBER(S)

12. DISTRIBUTION / AVAILABILITY STATEMENT

DISTRIBUTION STATEMENT A: Approved for public release; distribution is unlimited.

13. SUPPLEMENTARY NOTES

*Howard University, **Uninversity of South Florida, +Fayetteville State University, ++Nova Research, Inc.; *+NRL HBCU Interns

14. ABSTRACT

This report is related to an effort that seeks to develop autonomous sensors for environmental monitoring of changes in bacterial populations. The approach uses porphyrin modified antimicrobial peptides to produce colorimetric signatures, enabling the use of devices originally developed for chemical sensing applications. Here, we describe initial work focused on development of the covalent porphyrin-peptide constructs and the evaluation of those materials in the presence and absence of bacterial targets in aqueous solution

15. SUBJECT TERMS

environmental sensor, biosensor, colorimetric, porphyrin
antimicrobial peptide

16. SECURITY CLASSIFICATION OF:			**17. LIMITATION OF ABSTRACT**	**18. NUMBER OF PAGES**	**19a. NAME OF RESPONSIBLE PERSON**
a. REPORT	**b. ABSTRACT**	**c. THIS PAGE**			Brandy J. White
Unclassified Unlimited	Unclassified Unlimited	Unclassified Unlimited	Unclassified Unlimited	39	**19b. TELEPHONE NUMBER** *(include area code)* (202) 404-6100

This page intentionally left blank.

CONTENTS

FIGURES

TABLES

EXECUTIVE SUMMARY

In October 2012, the Center for Bio/Molecular Science and Engineering at the Naval Research Laboratory (NRL) began an effort intended to develop porphyrin modified antimicrobial peptides for application to colorimetric detection of bacterial threats. The goal was to apply the spectrophotometric characteristics of porphyrins and/or metalloporphyrins for indication of changes in the conformation of antimicrobial peptides upon interaction with targets. These covalent constructs would be used in an array format, and the relative responses of the materials would be applied to detection and discrimination of bacterial species in environmental air samples. This report addresses a component of the initial indicator development effort, focusing on the use of two different porphyrin structures in preparation of the materials.

This page intentionally left blank.

COLORIMETRIC ENVIRONMENTAL SENSOR: PORPHYRIN VARIATIONS

INTRODUCTION

In October 2012, the Center for Bio/Molecular Science and Engineering at the Naval Research Laboratory (NRL) began an effort intended to develop porphyrin modified antimicrobial peptides for application to colorimetric detection of bacterial threats. The goal was to apply the spectrophotometric characteristics of porphyrins and/or metalloporphyrins for indication changes in the conformation of antimicrobial peptides upon interaction with targets. These covalent constructions would be used as an array and the relative responses of the materials would be applied to detection and discrimination of bacterial species in environmental air samples. This report addresses a component of the initial indicator development effort, focusing on the linkage between the porphyrin and antimicrobial peptide components.

Antimicrobial peptides (AMPs) are a group of biomolecules that have evolved to recognize and kill target microbes by binding to and disrupting cell membranes (Figure 1). Several unique characteristics of AMPs make them extremely attractive alternatives to antibodies for detection of microbial biothreats: resistance to proteases, stability to environmental extremes, and high affinity, overlapping (but not identical) binding reactions with microbial membranes and membrane components. Arrays of AMPs have been used to detect and classify microbial pathogens with similar or superior sensitivity to antibody-based assays; their broad-spectrum binding activities also provide the potential for detection of unknown (or unsuspected) microbes. [1, 2, 3, 4, 5] In prior work, the AMP mediated target binding utilized an additional optical "tracer" (e.g., labeled antibody, non-specific dye) for signal transduction. This constraint increases the number of reagents required and the overall complexity of assays. Development of an AMP-based material that is capable of both recognition and signal generation without addition reagents or steps is highly desirable. This type of construct would provide greatly enhanced potential for application of AMP-based detection techniques to autonomous/distributed sensing platforms.

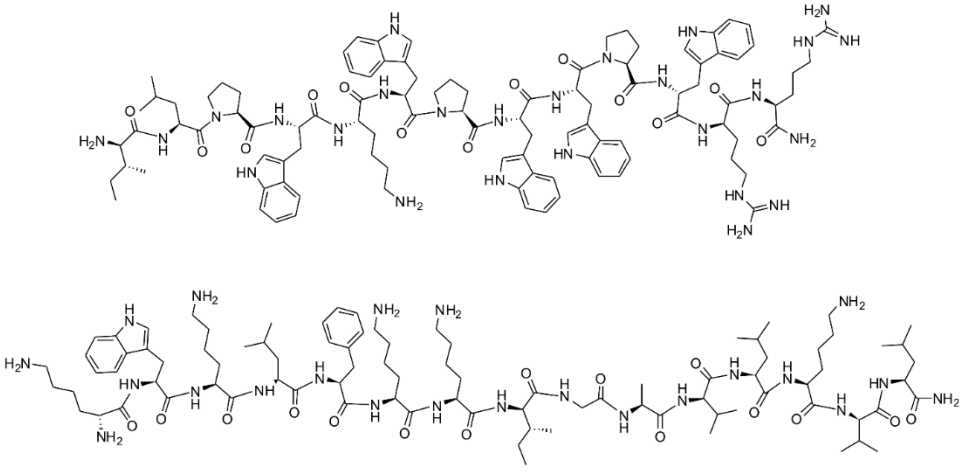

Fig. 1 – Examples of antimicrobial peptide structures: (top) indolicidin, (bottom) cecropin A (1-7) –melittin (2-9) hybrid.

Prior reports have described modification of porphyrin structures using single amino acids or dipeptides. [6, 7, 8] Changes in porphyrin fluorescence induced by binding of these constructs to proteins were observed. Our prior work described indicators developed to provide indication of bacterial presence without the need for additional reagents through utilization of changes in porphyrin spectrophotometric characteristics. [9] That work used a single porphyrin structure, 5-mono(4-carboxyphenyl)-10, 15, 20-

Manuscript approved October 3, 2018.

triphenyl porphyrin (C_1TPP), as part of the peptide constructs. Here, we report on the original four C_1TPP-peptides. In addition, we provide results for an additional C_1TPP construct and three constructs that incorporate an alternative porphyrin structure (Figure 2). The peptides considered include indolicidin (Indol), cecropin A (1-7) -melittin (2-9) hybrid (CeMe(S)), cecropin A (1-8) –melittin (1-18) hybrid (CeMe(L)), bactenecin, and Polymyxin E. Variations in performance noted within this set of eight indicator constructs are discussed.

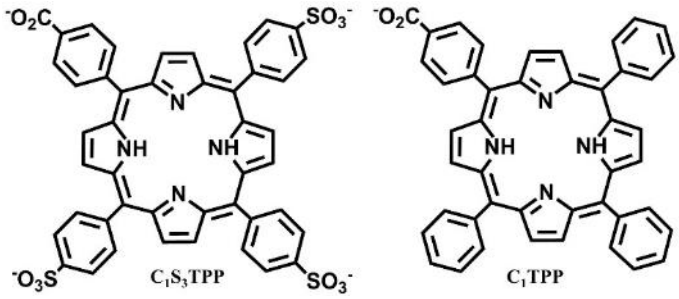

Fig. 2 – Porphyrin structures: meso-tri(4-sulfonatophenyl)mono(4-carboxyphenyl) porphyrin (C_1S_3TPP) and 5-mono(4-carboxyphenyl)-10, 15, 20-triphenyl porphyrin (C_1TPP).

METHODS

5-Mono(4-carboxyphenyl)-10, 15, 20-triphenyl porphine (C_1TPP) and meso-tri(4-sulfonatophenyl)mono(4-carboxyphenyl) porphyrin (C_1S_3TPP) were obtained from Frontier Scientific (Logan, UT; Figure 2). Vanadium (III) bromide, zinc chloride, cobalt (II) chloride, and dimethylsufloxide (DMSO) were obtained from Sigma-Aldrich (St. Louis, MO). 1-Ethyl-3-(3-dimethylaminopropyl) carbodiimide hydrochloride (EDC), N-hydroxysuccinimidyl ester (NHS) and sulfo-NHS were purchased from Pierce Thermo Scientific (Rockland, IL). Antimicrobial peptides indolicidin (Indol), bactenecin (Bac), cecropin A (1-8)-melittin (1-18) hybrid peptide (CeMe(L)), and cecropin A (1-7) –melittin (2-9) hybrid (CeMe(S)) were purchased from American Peptide Company (Sunnyvale, CA); polymyxin E (PME) was obtained from Sigma-Aldrich. Sequences are provided in Table 1.

Table 1. Antimicrobial peptides and amino acid sequences

Peptide	**Amino Acid Sequence**
Indolicidin (Indol)	ILPWKWPWWPWRR-NH_2
cecropin A-melittin hybrid, S-version (CeMe(S))	KWKLFKKIGAVLKVL-NH_2
cecropin A (1-8)-melittin (1-18) hybrid peptide (CeMe(L))	KWKLFKKIGIGAVLKVLTTGLPALIS-NH_2
Bactenecin (Bac)	RLCRIVVIRVCR; peptide is cyclized via sulfide bridge
Polymyxin E (PME)	Fatty acid chain – BTBBBLLBBT, B = diaminobutyrate; peptide is cyclized via side chain of B4

Direct covalent attachment of C_1TPP to the above peptides was accomplished under anhydrous conditions with carbodiimide-mediated coupling. Stock solutions of C_1TPP, EDC, NHS, bactenecin, and indolicidin were prepared in absolute ethanol prior to mixing; as neither PME nor CeMe(L) is highly soluble in absolute ethanol, stock solutions of these peptides were prepared in 4:1 (v/v) ethanol:acetonitrile. The composition of the reaction mixtures (molar equivalents) for C_1TPP constructs with CeMe(L) and CeMe(S) were as follows: 1 peptide: 1.1 porphyrin: 1.2 EDC: 1.2 NHS. In the case of the C_1S_3TPP constructs, compositions were: 1 peptide: 2.5 porphyrin: 5 EDC: 5 NHS for CeMe(S) and 1 peptide: 1 porphyrin: 5 EDC: 5 NHS for Indol. The Indol reaction was completed in 50 mM MES buffer pH 6 (aqueous conditions). After completion of the coupling reaction (>>2 hours), reaction mixtures were diluted with water and dialyzed (2000 molecular weight cutoff) exhaustively against water and phosphate-buffered saline (PBS). Construct concentrations are estimated based on the initial concentration of AMP and the total final volume of the preparation. Metal variants were prepared through incubation of porphyrin-AMP constructs (25 μM) with metal salts (vanadium (III) bromide; zinc chloride; cobalt (II) chloride; 50 μM) in aqueous

solution. [10] The solutions were thoroughly mixed and stored at 4ºC for at least 48 h. Metal incorporation was evaluated based on changes in absorbance and fluorescence characteristics. Construct names are abbreviated to indicate the metal, porphyrin, and AMP used; for example, CoC_1TPP-Indol is the cobalt variant of C_1TPP conjugated to the indolicidin peptide.

The bacterial targets for binding studies, *Escherichia coli* (XL1 blue) and *Bacillus cereus* (ATCC 10987), were grown to mid-log in Luria (37°C) or tryptic soy broth (30°C), respectively, before harvesting by centrifugation at 2800 × g for 10 min (4°C). Cell pellets were washed twice with phosphate-buffered saline (PBS), pH 7.4 and resuspended in 1/5 original volume of PBS. Cell numbers (in PBS) were then counted by flow cytometry (Accuri C6). Cell suspensions not used immediately were diluted with an equal volume of 60% glycerol in PBS before storage at -20°C. Prior to analysis, cells were diluted in PBS to the appropriate concentrations.

A Tecan XSafire microtiter plate reader was used to measure the absorbance and fluorescence of the porphyrin-AMP constructs in the presence and absence of bacterial targets. Absorbance was measured from 360 to 800 nm in steps of 2 nm. Fluorescence emission spectra were collected from 500 to 800 nm (2 nm steps) using 415 nm excitation while fluorescence excitation spectra were collected from 385 to 619 nm (2 nm steps) at 730 nm emission. In both cases, a gain of 160 was applied with 50 flashes at 400 Hz, and an integration time of 20 μs was employed. All experiments were conducted in 15% DMSO in order to ensure a homogeneous solution; porphyrin-AMP constructs have low water solubility due to the hydrophobicity of the porphyrin utilized and inherent solubilities of the AMPs. Cell concentrations ranging from 10^3 to 10^7 cells/mL were employed. Indicator concentrations were varied from 0.1 to 12 μM. In all cases, difference spectra were calculated as the point-by-point subtraction of indicator only spectra from spectra collected for the indicator in the presence of the target.

Fluorescence spectra for cell pellets utilized a total initial volume of 765 μL with 8 μM indicator and varying target cell concentrations in an Eppendorf tube (1.5 mL). As above, all experiments were conducted in 15% DMSO. The fluorescence of the initial solution was measured before centrifuging at 7,500 rpm for 10 min. Supernatant was then removed (665 μL), and the remaining solution and pellet were mixed thoroughly to resuspend components. The fluorescence of both the resulting supernatant and the resuspended pellet were collected using the microtiter plate protocol described above.

RESULTS

The goal in generation of porphyrin-modified AMPs is to provide a construct capable of detecting and discriminating between multiple bacterial species, in which the AMP component serves as a target recognition "domain" while the porphyrin component provides a mechanism of signal generation; specifically, the spectrophotometric characteristics of the porphyrin are impacted by structural changes in the antimicrobial peptide upon binding of the target. Direct interaction of a porphyrin with the bacterial target may result in changes to the spectrophotometric characteristics, but these will likely be nonspecific. With this in mind, the interaction of the porphyrin (C_1TPP) with the bacterial targets was first evaluated. No concentration dependent changes in the spectrophotometric characteristics of the porphyrin were noted upon interaction with either *E. coli* or *B. cereus*. An overall quench was noted in the fluorescence emission spectra of the porphyrin in the presence of bacterial cells (Appendix A); dose dependence was not observed.

Initial C_1TPP-AMP constructs.

Many, but not all AMPs, undergo a change in structure when interacting with target cells and membranes. In order to evaluate whether binding-mediated changes in an AMP's secondary structures would elicit a corresponding change in porphyrin spectrophotometric properties, we selected four cationic

AMPs with different structures and interaction types. Two of the AMP structures are minimally affected by target binding and two undergo significant changes in secondary structure upon interaction with cells. The former include bactenecin (Bac), a small β-structured peptide restricted by cyclization [11] and polymyxin E (PME) another cyclized peptide possessing a fatty acyl tail. [12] In both cases, only minor changes in conformation occur upon target binding. On the other hand, indolicidin (Indol) and cecropin A-melittin hybrid (CeMe(L)) are extended/unstructured in aqueous solution and undergo significant changes when interacting with target. Indolicidin assumes an extended boat conformation, and CeMe(L) forms an amphipathic α-helix upon binding to target cells and membranes. [13] As shown in Figure 3, the absorbance characteristics of C_1TPP in solution are distinctly different from those of the C_1TPP-AMP constructs. The varying peak positions in both absorbance and fluorescence as well as differences in extinction coefficients and fluorescence emission tend to indicate unique interactions between the porphyrin and each of the AMPs. It should be noted that the water solubility of the porphyrin alone is low, requiring addition of 15% DMSO to achieve sufficient concentration for collection of spectra. The C_1TPP-Bac and C_1TPP-PME constructs have similar solubility limitations while the C_1TPP-Indol and C_1TPP-CeMe(L) constructs are more soluble.

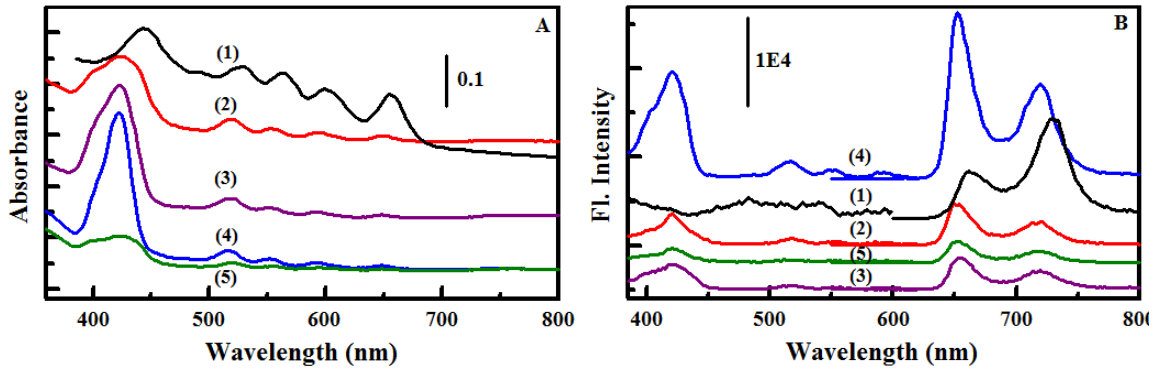

Fig. 3 – Porphyrin-modified peptides. Shown here are the absorbance (A) and fluorescence (B) spectra for C_1TPP and the C_1TPP-modified antimicrobial peptides: C_1TPP (1); C_1TPP-Bac (2); C_1TPP-Indol (3); C_1TPP-CeMe(L) (4); and C_1TPP-PME (5). All compounds in 15% DMSO at 20 μM.

When incubated in the presence of target bacteria, spectrophotometric changes for these porphyrin-AMP constructs were specific and dependent on the construct considered, the type of bacteria, and the concentrations of the two components. Figure 4 presents difference spectra for C_1TPP-Indol upon interaction with the two bacterial targets showing a peak/trough pair. While changes in absorbance for the Soret region were noted at similar peak positions, the concentration dependence of the interaction was different for the two types of bacteria (Figure 4; Appendix A). Changes in the absorbance spectrum were of larger intensity for the interaction of C_1TPP-Indol with *E. coli* than those observed for the interaction with *B. cereus*. Changes in the fluorescence of the construct were also noted upon interaction with the targets with both targets yielding similar behavior (Appendix A).

The interaction of C_1TPP-CeMe(L) with the two bacterial targets produced results that were distinct from those observed for C_1TPP-Indol in both the absorbance and fluorescence spectra. For both bacterial targets, only a trough was observed in the Soret region of the absorbance spectrum, centered at 420 nm (Figure 5). The changes in fluorescence for the interaction of the two targets with C_1TPP-CeMe(L) were small (Appendix A). Constructs comprised of C_1TPP with Bac or PME – the two peptides offering minimal structural rearrangements upon target binding – showed no significant changes in absorbance at any of the evaluated concentrations (Appendix A). Slight changes in fluorescence were noted for only the highest concentrations of C_1TPP-PME (20 μM) and targets (1.6×10^7 cell/mL) used; changes were below the threshold needed for effective evaluation. These changes in spectrophotometric character may be related to indicator solubility rather than specific interactions.

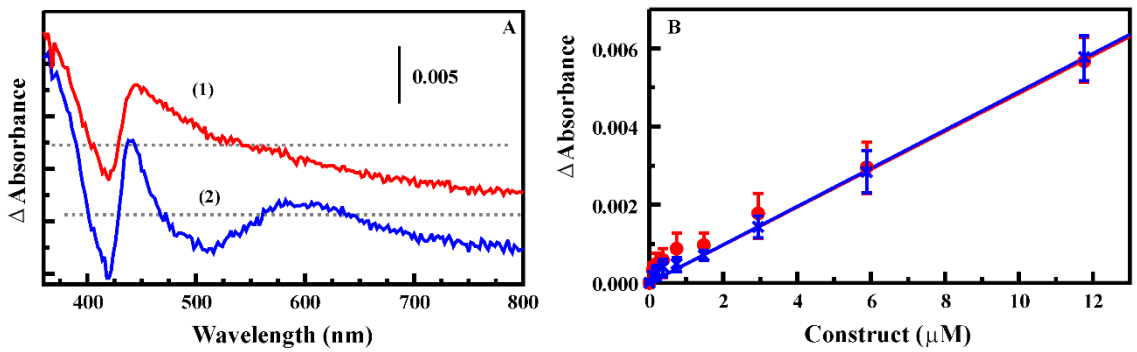

Fig. 4 – Interaction of C_1TPP-Indol with bacterial cells. Absorbance difference spectra (A) are calculated as the point-by-point subtraction of the spectrum of the construct alone (20 μM) from that of the construct in the presence of target (i.e., C_1TPP-Indol + *E. coli* minus C_1TPP-Indol): *E. coli* (1) and *B. cereus* (2) at 2.4×10^5 cell/mL. Also shown is the concentration dependence (B) of the intensity changes: *E. coli* (x, 1.9×10^6 cell/mL) and *B. cereus* (circle, 3.8×10^6 cell/mL).

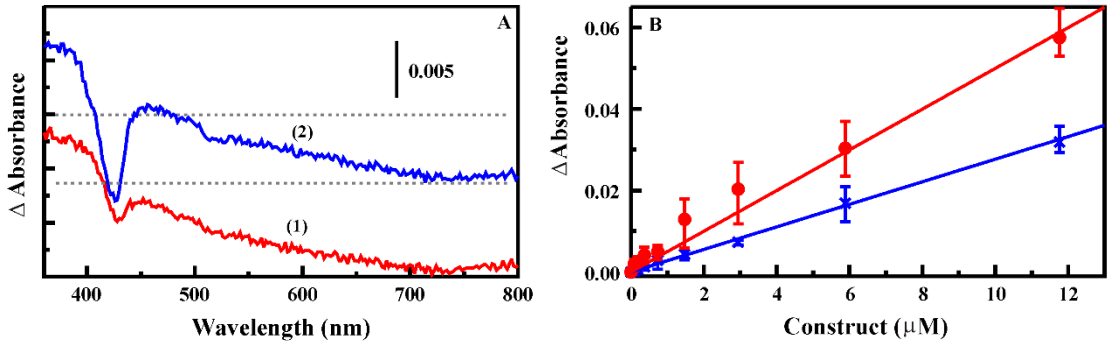

Fig. 5 - Interaction of C_1TPP-CeMe(L) with bacterial cells. Absorbance difference spectra (A) are calculated as the point-by-point subtraction of the spectrum of the construct alone (20 μM) from that of the construct in the presence of target (i.e., C_1TPP-CeMe(L) + *E. coli* minus C_1TPP-CeMe(L)): *E. coli* (1) and *B. cereus* (2) at 1.6×10^5 cell/mL. Also shown is the concentration dependence (B) of the intensity changes. Error bars indicate the range of values obtained for replicate measurements.

An additional experiment was designed, in order to identify interactions between the porphyrin-peptide constructs and targets. In the above experiments, interaction can be determined based only on impact on spectrophotometric characteristics of the porphyrin. Minimal changes in absorbance/fluorescence could indicate that conjugation to the porphyrin caused a change in the interaction between the antimicrobial peptide and the cell, i.e. no binding. These types of changes in binding behavior have been reported previously upon conjugation to surfaces.[4] Alternatively, the structural changes in the antimicrobial peptide occurring upon interaction of the indicator with the bacterial targets may be insufficient to cause changes in the spectrophotometric characteristics of the porphyrins. This could result from orientation of the porphyrin to the peptide or distance between structural rearrangements and the porphyrin. In order to further explore possible interactions between constructs and targets, targets and indicators were mixed in microcentrifuge tubes. Fluorescence was evaluated for this initial solution as well as for the pellet and supernatant following centrifugation of the tube. Analysis was completed based on the ratio of the concentration in the pellet to that of the original solution as calculated based on peak fluorescence. This analysis does not rely on changes in the spectrophotometric characteristics of the porphyrin, rather it evaluates accumulation of the construct due to the presences of bacterial cells.

In a tube with no bacterial target, indicator concentrations in pellets containing C_1TPP-Bac were nearly identical to those of the initial solution (ratio = 1.01). The concentration of C_1TPP-Bac in the pellet increased (less indicator in the supernatant) as *B. cereus* concentration increased (Figure 6), indicating that C_1TPP-Bac was bound to, or was otherwise interacting with, the *B. cereus* cells; however, no increase in pellet concentrations was noticed in the presence of *E. coli*. C_1TPP-PME showed increasing pellet

concentration with increasing target concentration for both *E. coli* and *B. cereus*. There was also significant precipitation of the indicator from solution in the absence of target, likely owing to the more limited solubility of the C_1TPP-PME indicator.

Figure 6 includes data for C_1TPP-Indol and C_1TPP-CeMe(L) for comparison. Based on this analysis, it appears that there are interactions for C_1TPP-PME and C_1TPP-Bac indicators with *B. cereus* and that the C_1TPP-PME indicator interacts with *E. coli*. The lack of interactions between C_1TPP-Bac and *E. coli* would tend to indicate that the AMP structure has been impacted negatively by conjugation with the porphyrin given the fact that native (unconjugated) Bac does bind to *E. coli* cells. [11] In both cases, when the absorbance and fluorescence spectra of the target containing pellets are compared to normalized indicator only spectra, no significant changes are noted. It is likely that any structural changes occurring upon interaction of the indicators with the bacterial targets are insufficient to cause a change in the spectrophotometric characteristics of the porphyrins.

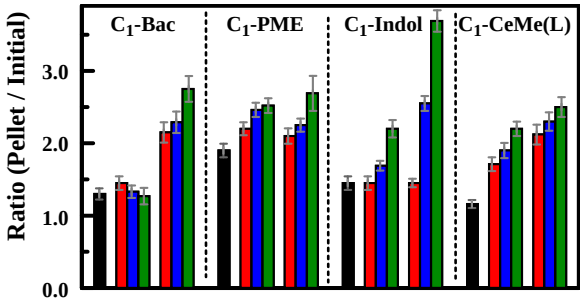

Fig. 6 - Pellet analysis. Ratio of peak fluorescence in the pellet following centrifuge to that of the initial target solution. For each indicator, the black bar indicates results in the absence of bacterial cells. The remaining bars are for initial bacteria concentrations (left to right) for *E. coli* at 1.9×10^4, 1.9×10^5, and 1.9×10^6 cell/mL and for *B. cereus* at 2.0×10^4, 2.0×10^5, and 2.0×10^6 cell/mL. Initial construct concentration is 8 μM in all cases.

Metal complexes.

Formation of metalloporphyrin variants strongly impacts both the spectrophotometric characteristics of the porphyrin and its interaction with the environment. It was thought that incorporation of metals into the porphyrin component of the constructs might produce a stronger response to changes in one or more of the constructs. Vanadium, cobalt, and zinc were used to generate metal complexes for the four constructs considered here. Metal incorporation was evaluated based on changes in the fluorescence and absorbance characteristics of the constructs. In all cases, changes in the shape, intensities, and locations of peaks were noted. Figure 7 presents results for C_1TPP-Indol as an example (additional results in Appendix A). Here, quenching of the fluorescence intensity is noted for the vanadium and cobalt variants, and the zinc construct shows a significant shifts both absorbance and fluorescence. The absorbance spectra show changes in intensity for all of the metal variants with changes in relative intensities across the resulting spectra.

The absorbance and fluorescence characteristics of each of the metal-modified constructs were measured in the presence and absence of varying concentrations of *E. coli* and *B. cereus*. The changes in the spectrophotometric characteristics were distinct for each of the metal complexes of C_1TPP-Indol (example in Figure 8; additional results in Appendix A). Concentration dependence based on the absorbance spectra indicated that the vanadium version of the construct yielded the largest changes in absorbance (Figure 7 and Appendix A) with changes in fluorescence insufficient for analysis. The zinc version of the construct provided significant changes in both absorbance and fluorescence. Given these results, selection of a candidate construct may depend on the application desired, whether utilizing absorbance, fluorescence, or reflectance based interrogation.

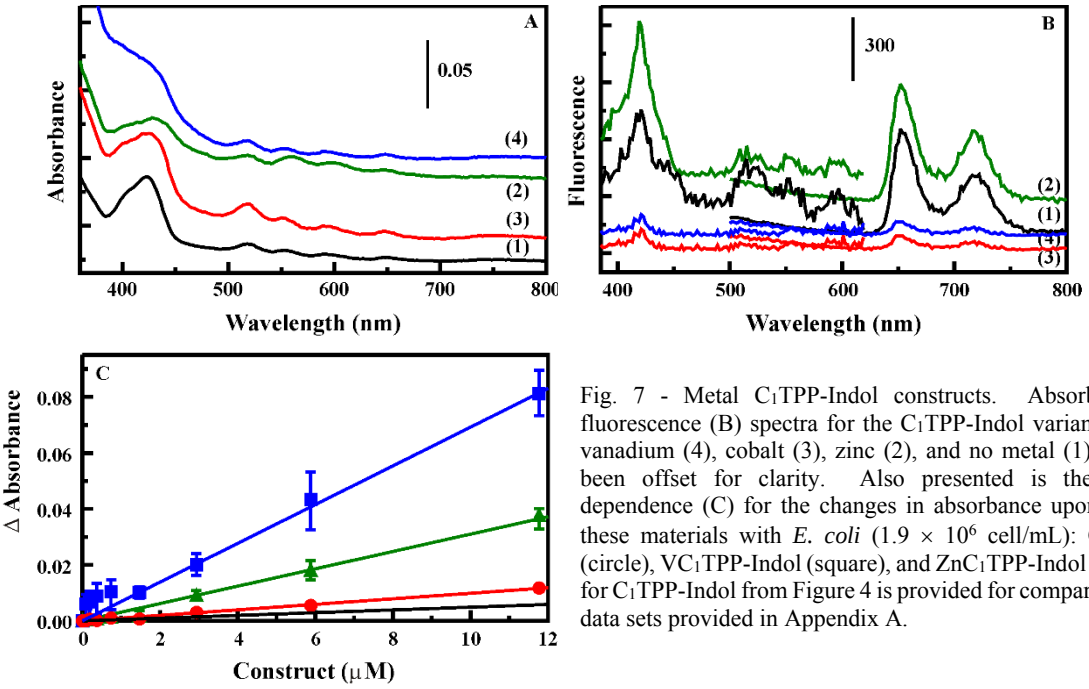

Fig. 7 - Metal C_1TPP-Indol constructs. Absorbance (A) and fluorescence (B) spectra for the C_1TPP-Indol variants (8 μM) with vanadium (4), cobalt (3), zinc (2), and no metal (1). Spectra have been offset for clarity. Also presented is the concentration dependence (C) for the changes in absorbance upon interaction of these materials with *E. coli* (1.9×10^6 cell/mL): CoC_1TPP-Indol (circle), VC_1TPP-Indol (square), and ZnC_1TPP-Indol (triangle). A fit for C_1TPP-Indol from Figure 4 is provided for comparison. Complete data sets provided in Appendix A.

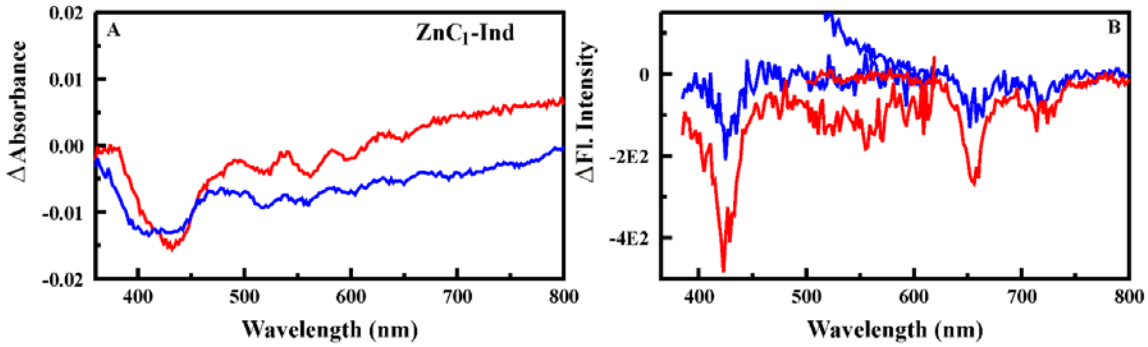

Fig. 8 - ZnC_1TPP-Indol construct. Absorbance (A) and fluorescence (B) difference spectra for the interaction of ZnC_1TPP-Indol (all at 12 μM) with *E. coli* (red; 1.9 x10^6 cell/mL) and *B. cereus* (blue; 2.0 x10^6 cell/mL).

Changes in absorbance upon formation of the C_1TPP-CeMe(L) metal complexes were broad and less well defined than those observed for the C_1TPP-Indol construct (Appendix A). It is possible that incomplete metal complex formation was achieved in this case. Additional incubation time did not result in additional spectrophotometric changes. Based on the data collected, the non-metal C_1TPP-CeMe(L) shows larger changes in both absorbance and fluorescence upon interaction with targets than any of the metal variants (Appendix A). Metal incorporation was evaluated in the PME and Bac (Appendix A) constructs to assess the possibility that the sensitivity of the porphyrin could be increased leading to changes upon target interaction. This was not the case for these constructs. No significant changes in fluorescence or absorbance were noted for any of the Bac or PME variants (Appendix A).

Additional C_1TPP construct.

Cecropin A (1-7) -melittin (2-9) hybrid (CeMe(S)) is a shorter variant of the CeMe(L) peptide used originally. While the shorter peptide is more highly charged on a per-mole basis, the longer variant has an amphipathic extension with three residues capable of hydrogen bonding. As in the case of the longer variant, CeMe(S) is expected to change conformation upon interaction with targets, although the nature of the structural changes will likely differ from CeMe(L). A C_1TPP-CeMe(S) construct was synthesized. Figure 9 presents the spectrophotometric characteristics of this construct along with those of the C_1TPP-CeMe(L) and C_1TPP-Indol. The absorbance and fluorescence for C_1TPP-CeMe(S) are distinct from the characteristics observed for the other materials with more broadening of the Soret noted.

The interaction of the C_1TPP-CeMe(S) construct with the targets produced minimal changes in the absorbance and fluorescence spectra of the porphyrin. No changes in absorbance were noted when incubated with *B. cereus*. Changes upon interaction with *E. coli* were significantly smaller than those noted for the C_1TPP-CeMe(L) construct. Changes in fluorescence on interaction with the targets were also smaller than those noted for the C_1TPP-CeMe(L) construct. There was, however, concentration dependence noted.

As with the original porphyrin-peptide constructs, target cells and indicators were mixed in microcentrifuge tubes in order to explore possible interactions. Spectrophotometric characteristics were evaluated for this initial solution as well as for the pellet and supernatant following centrifugation of the tube. Analysis was completed based on the ratio of the concentration in the pellet to that of the original solution as calculated based on peak absorbance or fluorescence. In a tube with no bacterial target, fluorescence analysis indicated concentrations in pellets containing C_1TPP-CeMe(S) were similar to those of the initial solution (ratio = 0.93). The concentration of C_1TPP-CeMe(S) in the pellet was increased slightly by the presence of *E. coli* or *B. cereus* (Figure 11); however, the increases were less significant than those noted for C_1TPP-CeMe(L) in the presence of the targets. Changes in binding behavior have been reported previously upon conjugation to surfaces. [4] It is possible, based on the results presented here, that conjugation to C_1TPP has negatively impacted the interaction between CeMe(S) and the cells.

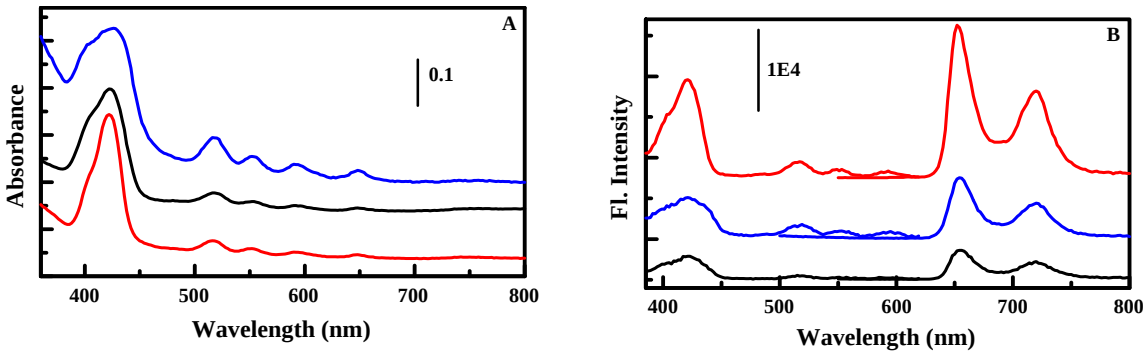

Fig. 9 – C_1TPP-CeMe(S) construct. Absorbance (A) and fluorescence (B) spectra for C_1TPP-Indol (black); C_1TPP-CeMe(L) (red); C_1TPP-CeMe(S) (blue). Indicators at 20 μM in 15% DMSO. Complete data sets provided in Appendix C.

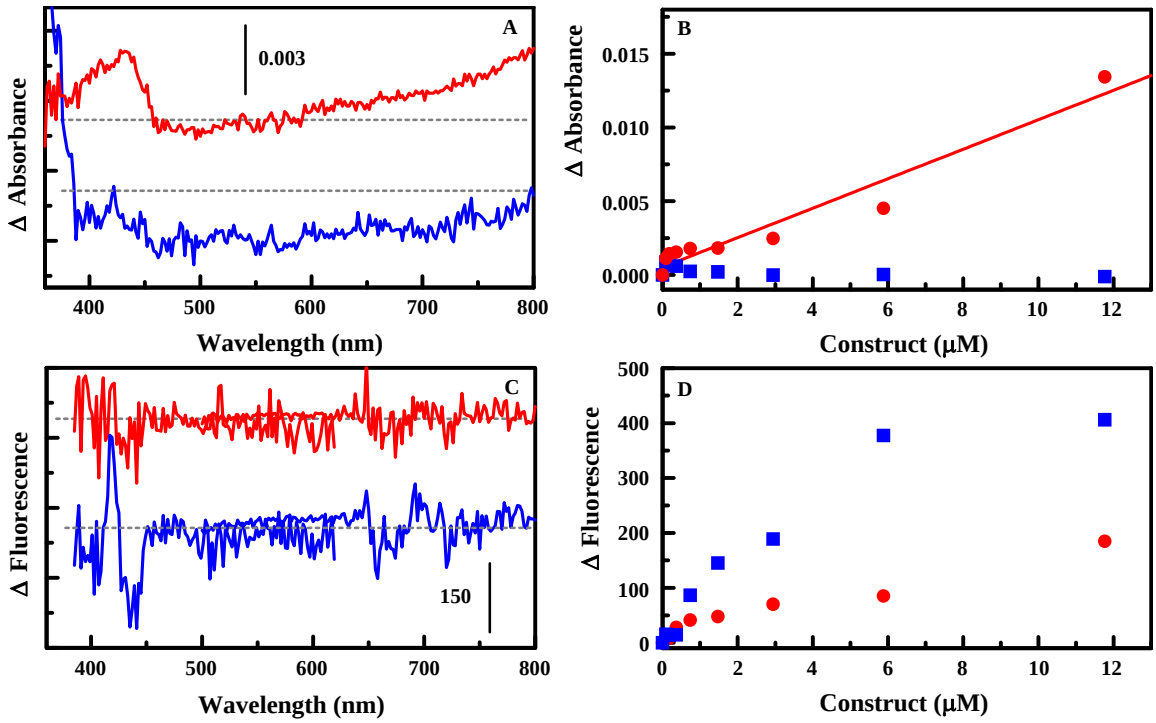

Fig. 10 – C_1TPP-CeMe(S) construct. Absorbance (A) and fluorescence (C) difference spectra for the interaction of C_1TPP-CeMe(S) (indicator 11.8 μM) with *E. coli* (red; 1.9×10^6 cell/mL) and *B. cereus* (blue; 2.0×10^6 cell/mL). The concentration dependence of these changes is presented in Panels B and D. Complete data sets provided in Appendix C.

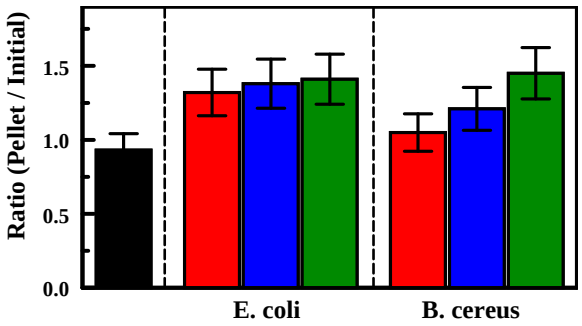

Fig. 11 - Pellet analysis for C_1TPP-CeMe(S). Ratio of peak fluorescence in the pellet following centrifuge to that of the initial target solution. For each indicator, the black bar indicates results in the absence of bacterial cells. The remaining bars are for bacterial concentrations (left to right) for *E. coli* at 1.9×10^4, 1.9×10^5, and 1.9×10^6 cell/mL and for *B. cereus* at 2.0×10^4, 2.0×10^5, and 2.0×10^6 cell/mL. Initial construct concentration is 11.8 μM in all cases.

C_1S_3TPP constructs.

Indol, CeMe(S), and CeMe(L) peptides were modified with C_1S_3TPP using the same chemistry as that applied in synthesis of the C_1TPP constructs. C_1S_3TPP is a more hydrophilic porphyrin with sulfonate groups on the periphery in addition to the single carboxylic acid group (Figure 2), and therefore, the resulting C_1S_3TPP -peptide constructs are more hydrophilic than the C_1TPP versions. As shown in Figure 12, the absorbance and fluorescence excitation spectra are sharper than those of the C_1TPP. These constructs also show higher fluorescence intensities than those of the C_1TPP analogs.

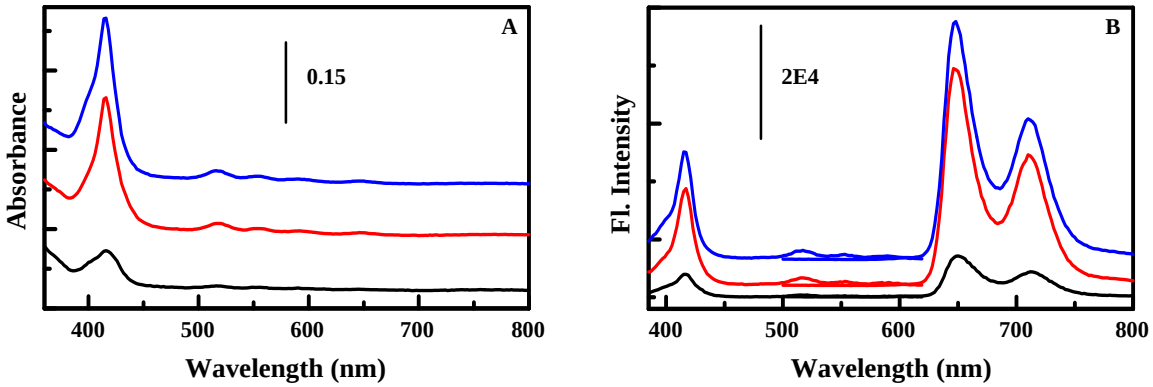

Fig. 12 – C_1S_3TPP constructs. Absorbance (A) and fluorescence (B) spectra for C_1S_3TPP-Indol (black); C_1S_3TPP-CeMe(L) (red); C_1S_3TPP-CeMe(S) (blue). Indicators at 11.8 μM in 15% DMSO. Complete data sets provided in Appendix D.

The interaction of the C_1S_3TPP-Indol construct with the targets produced significant and highly similar changes in absorbance (Figure 13; additional data Appendix D). Fluorescence spectra show more noise than expected, but concentration dependent changes were sufficient for analysis (Figure 13). The C_1S_3TPP-CeMe(L) construct also produced significant changes in absorbance when incubated with the targets (Figure 14). Changes in fluorescence were also pronounced and concentration dependent. Changes in the spectrophotometric characteristics were the same regardless of the bacterial target used. Similar to the C_1TPP-CeMe(S) construct, exposure of the C_1S_3TPP-CeMe(S) indicator to bacteria produced significant changes in absorbance only at the highest target concentrations (Figure 15). Changes in fluorescence were also noted only for the highest concentrations and were the same regardless of the bacterial target used.

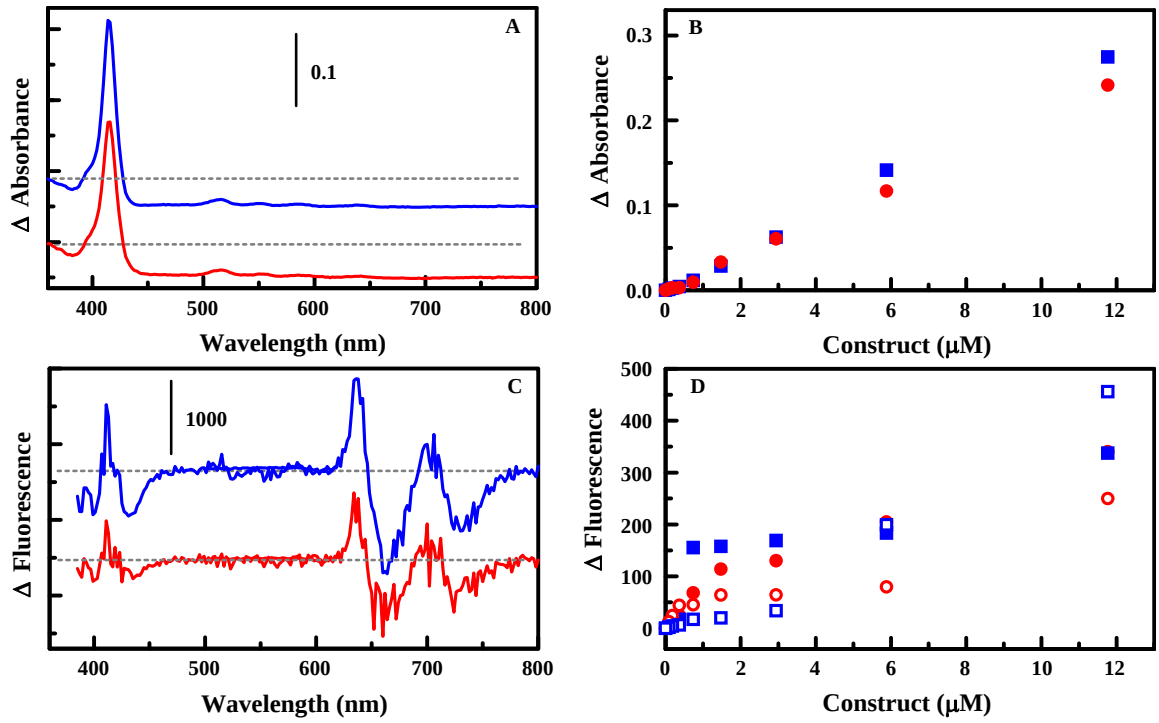

Fig. 13 – C_1S_3TPP-Indol construct. Absorbance (A) and fluorescence (C) difference spectra for the interaction of C_1S_3TPP-Indol (indicator 11.8 μM) with *E. coli* (red; 1.9×10^6 cell/mL) and *B. cereus* (blue; 2.0×10^6 cell/mL). The concentration dependence of these changes is presented in Panels B and D. Complete data sets provided in Appendix D.

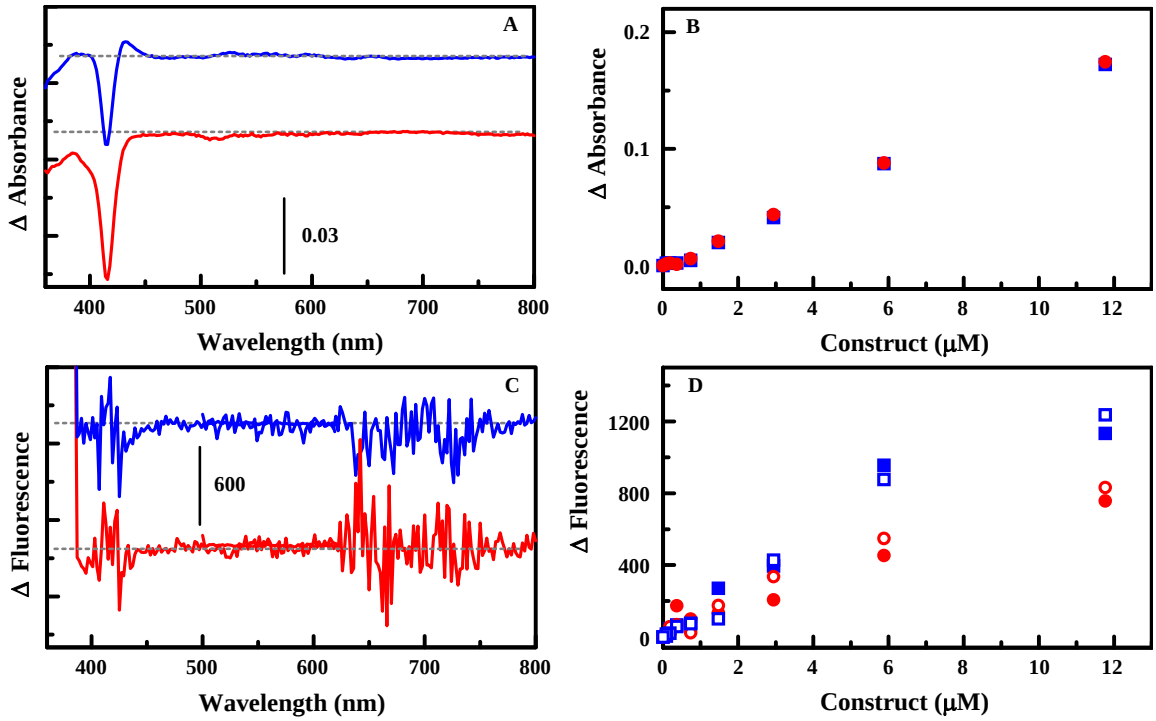

Fig. 14 – C_1S_3TPP-CeMe(L) construct. Absorbance (A) and fluorescence (C) difference spectra for the interaction of C_1S_3TPP-CeMe(L) (indicator 11.8 μM) with *E. coli* (red; 1.9×10^6 cell/mL) and *B. cereus* (blue; 2.0×10^6 cell/mL). The concentration dependence of these changes is presented in Panels B and D. Complete data sets provided in Appendix D.

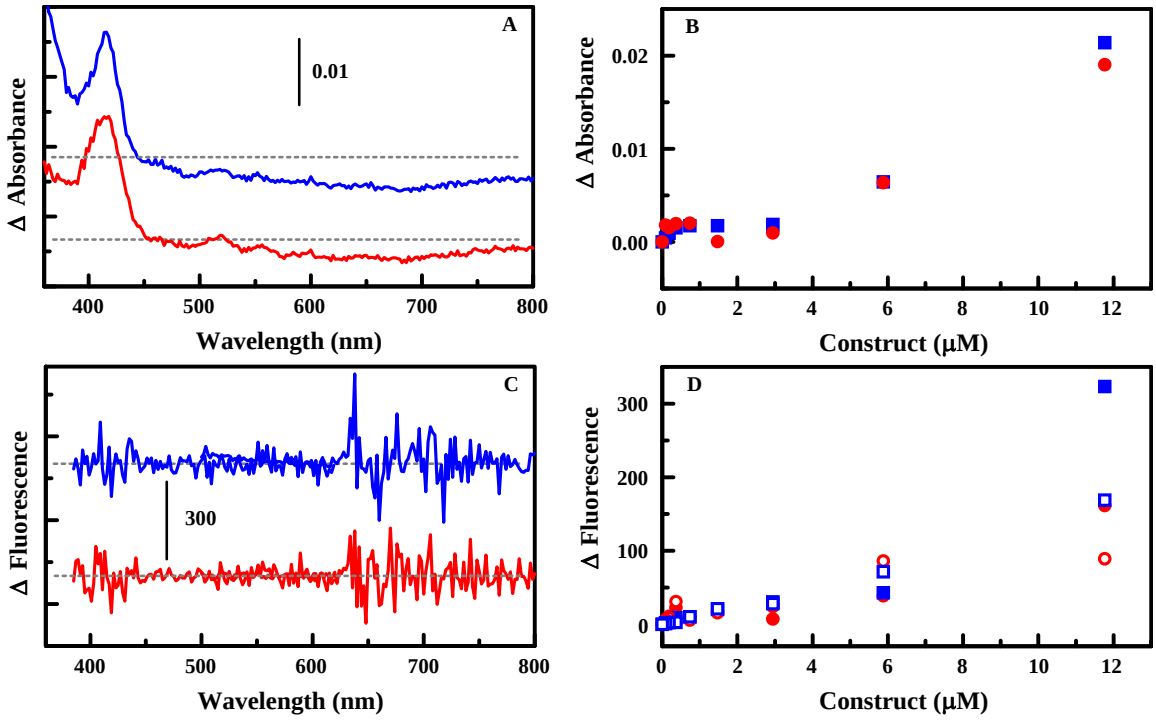

Fig. 15 – C_1S_3TPP-CeMe(S) construct. Absorbance (A) and fluorescence (C) difference spectra for the interaction of C_1S_3TPP-CeMe(S) (indicator 11.8 μM) with *E. coli* (red; 1.9×10^6 cell/mL) and *B. cereus* (blue; 2.0×10^6 cell/mL). The concentration dependence of these changes is presented in Panels B and D. Complete data sets provided in Appendix D.

In order to explore possible interactions, targets and indicators were mixed in microcentrifuge tubes. Spectrophotometric characteristics were evaluated for this initial solution as well as for the pellet and supernatant following centrifugation of the tube. Analysis was completed based on the ratio of the concentration in the pellet to that of the original solution as calculated based on peak absorbance or fluorescence. In a tube with no bacterial target, fluorescence analysis indicated concentrations in pellets containing C_1S_3TPP-Indol were similar to those of the initial solution (ratio = 1.06). The concentration of C_1S_3TPP-Indol in the pellet was increased by the presence of *E. coli* or *B. cereus* with *B. cereus* producing higher concentrations in the pellet (Figure 16).

In a tube with no bacterial target, fluorescence analysis indicated concentrations in pellets containing C_1S_3TPP-CeMe(L) or C_1S_3TPP-CeMe(S) were similar to those of the initial solution (ratios = 1.06 and 0.97, respectively). The concentration of C_1S_3TPP-CeMe(L) in the pellet was increased by the presence of *E. coli* or *B. cereus* with *B. cereus* producing higher concentrations in the pellet (Figure 16). However, the concentration of C_1S_3TPP-CeMe(S) in the pellet was increased by the presence of *B. cereus*, with *E. coli* producing changes only within the noise of the analysis (Figure 16). Changes in binding behavior of antimicrobial peptides have been reported previously upon conjugation to surfaces. [4] It is possible, based on the results presented here, that conjugation to C_1S_3TPP has negatively impacted the interaction between CeMe(S) and the cells. This is consistent with the behavior noted in the C_1TPP-CeMe(S) construct.

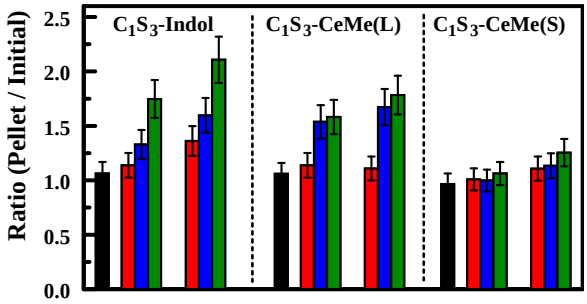

Fig. 16 - Pellet analysis for C_1S_3TPP-constructs. Ratio of peak fluorescence in the pellet following centrifuge to that of the initial target solution. For each indicator, the black bar indicates results in the absence of bacterial cells. The remaining bars are for bacterial concentrations (left to right) for *E. coli* at 1.9×10^4, 1.9×10^5, and 1.9×10^6 cell/mL and for *B. cereus* at 2.0×10^4, 2.0×10^5, and 2.0×10^6 cell/mL. Initial construct concentration is 11.8 μM in all cases.

CONCLUSIONS

We have demonstrated the potential of porphyrin modified antimicrobial peptides for indication of bacterial targets on the basis of changes in the spectrophotometric characteristics of the construct. Peptides offering little or no change in conformation upon target interaction did not result in constructs that demonstrated changes in absorbance or fluorescence when in the presence of *E. coli* or *B. cereus* (C_1-PME and C_1-Bac). Differing spectrophotometric changes were observed with the C_1TPP constructs that did undergo significant conformational changes (C_1TPP-CeMe(L) and C_1TPP-Indol). Formation of metal complexes with the porphyrin component of these constructs was shown to alter the spectrophotometric characteristics of the construct as well as the resulting absorbance and fluorescence changes noted upon interaction with a target. The C_1TPP-CeMe(S) construct was expected to change conformation upon interaction with the bacterial targets; however, the noted changes were minimal. Formation of C_1S_3TPP-Indol, -CeMe(L), and -CeMe(S) constructs produced results consistent with those of the C_1TPP constructs. Specific changes in the spectrophotometric characteristics were unique for each porphyrin-peptide combination.

The porphyrin-peptide constructs demonstrated here offer the potential to enable a new type of biosensing approach. Because the construct offers both target recognition and optical transduction, no additional reagents are necessary (e.g., labeled antibody or non-specific dye). The constructs in this study were utilized in solution, but we are currently working to immobilize the porphyrin-peptide constructs. An

immobilized array will enable use of these constructs with either fluorescence-based [14] or reflectance-based [15] detectors. As in previously described work, the response of an array of indicators can be utilized to classify the targets detected, [1, 16] where a single indicator would not provide sufficient information for identification or classification.

ACKNOWLEDGEMENTS

A. Gleaves and S. Monk participated in this effort through the Office of Naval Research supported HBCU internship program at NRL. E. Archibong was supported at the Naval Research Laboratory through NSF Florida-Georgia Louis Stokes Alliance for Minority Participation (FGLSAMP) Bridge to the Doctorate grant (HRD #1139850) & the Alfred P. Sloan Minority PhD program. This research was sponsored by the U.S. Office of Naval Research through Naval Research Laboratory base funds (69-6A26). The views expressed here are those of the authors and do not represent those of the U.S. Navy, the U.S. Department of Defense, or the U.S. Government.

REFERENCES

1. N.V. Kulagina; G.P. Anderson; F.S. Ligler; K.M. Shaffer; C.R. Taitt, "Antimicrobial peptides: New recognition molecules for detecting botulinum toxins," *Sensors* **7**, 2808-2824 (2007).
2. N.V. Kulagina; K.M. Shaffer; G.P. Anderson; F.S. Ligler; C.R. Taitt, "Antimicrobial peptide-based array for Escherichia coli and Salmonella screening," *Analytica Chimica Acta* **575**, 9-15 (2006).
3. M.M. Ngundi; N.V. Kulagina; G.P. Anderson; C.R. Taitt, "Nonantibody-based recognition: alternative molecules for detection of pathogens," *Expert Review of Proteomics* **3**, 511-524 (2006).
4. S.H. North; J. Wojciechowski; V. Chu; C.R. Taitt, "Surface immobilization chemistry influences peptide-based detection of lipopolysaccharide and lipoteichoic acid," *Journal of Peptide Science* **18**, 366-372 (2012).
5. C.R. Taitt; L.C. Shriver-Lake; M.M. Ngundi; F.S. Ligler, "Array Biosensor for Toxin Detection: Continued Advances," *Sensors* **8**, 8361-8377 (2008).
6. L. Baldini; A.J. Wilson; J. Hong; A.D. Hamilton, "Pattern-based detection of different proteins using an array of fluorescent protein surface receptors," *Journal of the American Chemical Society* **126**, 5656-5657 (2004).
7. L.K. Tsou; R.K. Jain; A.D. Hamilton, "Protein surface recognition by porphyrin-based receptors," *Journal of Porphyrins and Phthalocyanines* **8**, 141-147 (2004).
8. H.C. Zhou; L. Baldini; J. Hong; A.J. Wilson; A.D. Hamilton, "Pattern recognition of proteins based on an array of functionalized porphyrins," *Journal of the American Chemical Society* **128**, 2421-2425 (2006).
9. B.J. Johnson; C.R. Taitt; A. Gleaves; S.H. North; A.P. Malanoski; I.A. Leska; E. Archibong; S.M. Monk, "Porphyrin-modified antimicrobial peptide indicators for detection of bacteria," *Sens Biosensing Res* **8**, 1-7 (2016).
10. B.J. Johnson; N.E. Anderson; P.T. Charles; A.P. Malanoski; B.J. Melde; M. Nasir; J.R. Deschamps, "Porphyrin-Embedded Silicate Materials for Detection of Hydrocarbon Solvents," *Sensors* **11**, 886-904 (2011).
11. M.H. Wu; R.E.W. Hancock, "Interaction of the cyclic antimicrobial cationic peptide bactenecin with the outer and cytoplasmic membrane," *J. Biol. Chem.* **274**, 29-35 (1999).
12. P. Pristovsek; J. Kidric, "Solution structure of polymyxins B and E and effect of binding to lipopolysaccharide: An MMR and molecular modeling study," *J. Med. Chem.* **42**, 4604-4613 (1999).

13. F. Abrunhosa; S. Faria; P. Gomes; I. Tomaz; J.C. Pessoa; D. Andreu; M. Bastos, "Interaction and lipid-induced conformation of two cecropin-melittin hybrid peptides depend on peptide and membrane composition," *Journal of Physical Chemistry B* **109**, 17311-17319 (2005).
14. C.A. Rowe-Taitt; J.P. Golden; M.J. Feldstein; J.J. Cras; K.E. Hoffman; F.S. Ligler, "Array biosensor for detection of biohazards," *Biosensors & Bioelectronics* **14**, 785-794 (2000).
15. B.J. Johnson; J.S. Erickson; J. Kim; A.P. Malanoski; I.A. Leska; S.M. Monk; D.J. Edwards; T.N. Young; J. Verbarg; C. Bovais; R.D. Russell; D.A. Stenger, "Miniaturized reflectance devices for chemical sensing," *Meas Sci & Tech* **25**, 095101 (2014).
16. C.R. Taitt; S.H. North; N.V. Kulagina, "Antimicrobial peptide arrays for detection of inactivated biothreat agents," *Methods in Molecular Biology* **570**, 233-255 (2009).

APPENDIX A

ADDITIONAL DATA & ANALYSIS FOR INITIAL C_1TPP CONSTRUCTS

Figure A1. Interaction of C_1TPP with bacteria. Absorbance and fluorescence spectra for the C_1TPP (6 μM) in the presence and absence (black) of bacterial cells (1.8×10^6): *E. coli* (red) and *B. cereus* (blue).

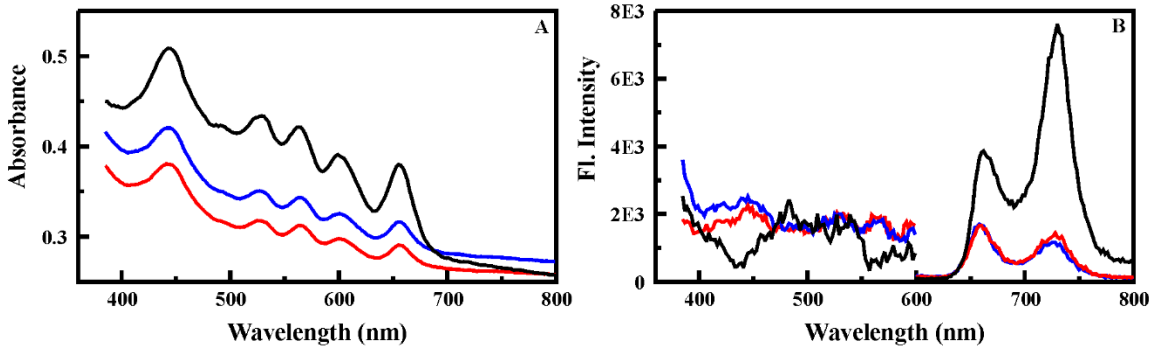

Figure A2. Interaction of C_1-Indol with bacteria. Fluorescence spectra (A) for C_1-Indol (20 μM) in the presence and absence (black) of bacterial cells (1.6×10^6): *E. coli* (red) and *B. cereus* (blue). Difference spectra are also presented (B).

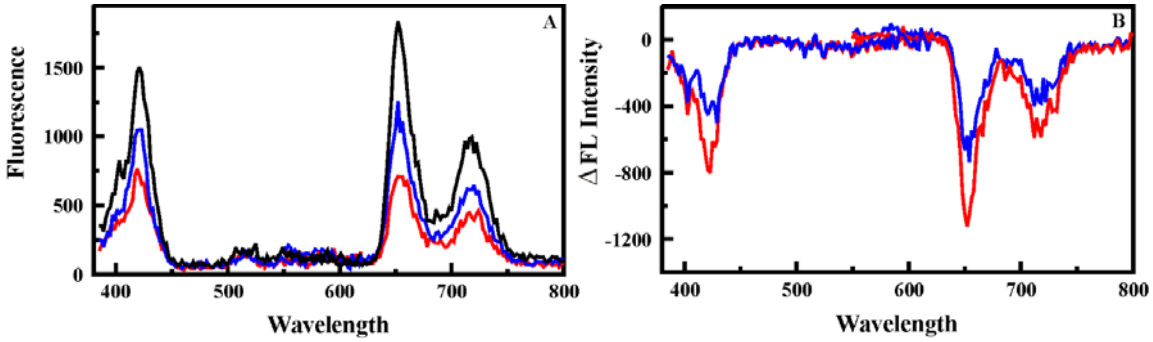

Figure A3. Interaction of C_1-CeMe with bacteria. Fluorescence spectra (A) for C_1-CeMe (20 μM) in the presence and absence (black) of bacterial cells (1.8×10^6 cell/mL): *E. coli* (red) and *B. cereus* (blue).

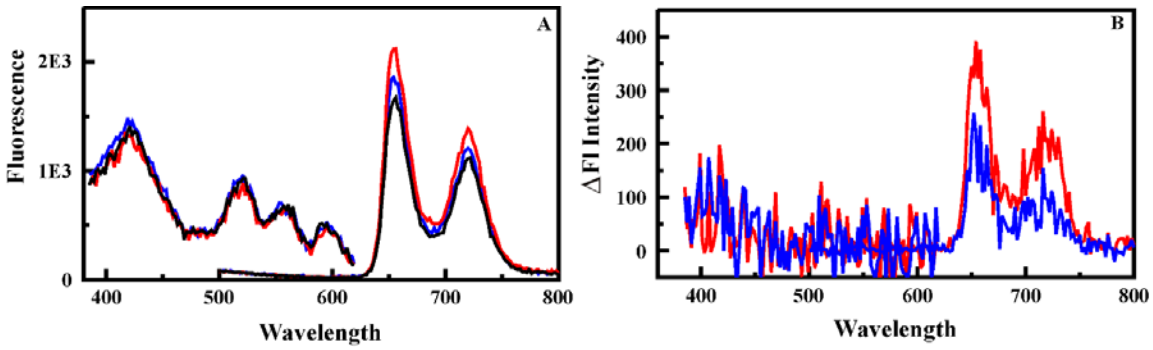

Figure A4. Interaction of C_1-Bac with bacteria. Absorbance (A) and fluorescence (B) difference spectra for C_1-Bac (11.9 μM) in the presence and absence (black) of bacterial cells (1.9×10^6 cell/mL): *E. coli* (red) and *B. cereus* (blue).

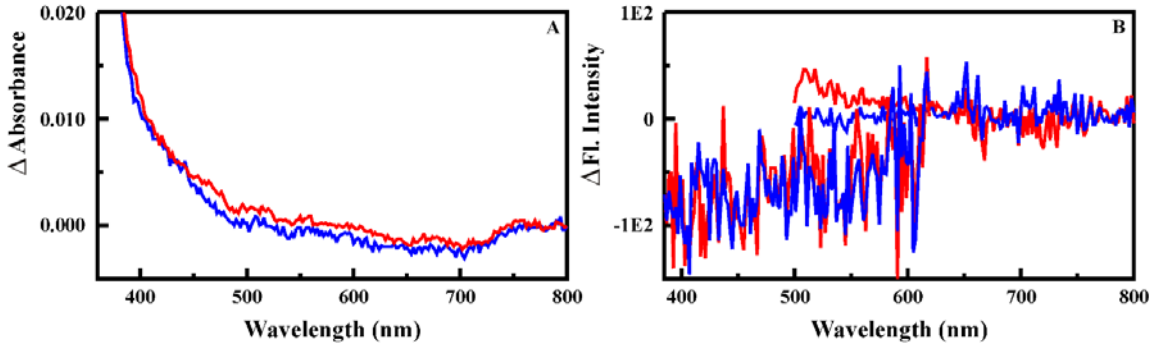

Figure A5. C_1-PME construct. Absorbance and fluorescence difference spectra for the interaction of C_1-PME (11.9 μM) in the presence and absence (black) of bacterial cells (1.9×10^6 cell/mL): *E. coli* (red) and *B. cereus* (blue).

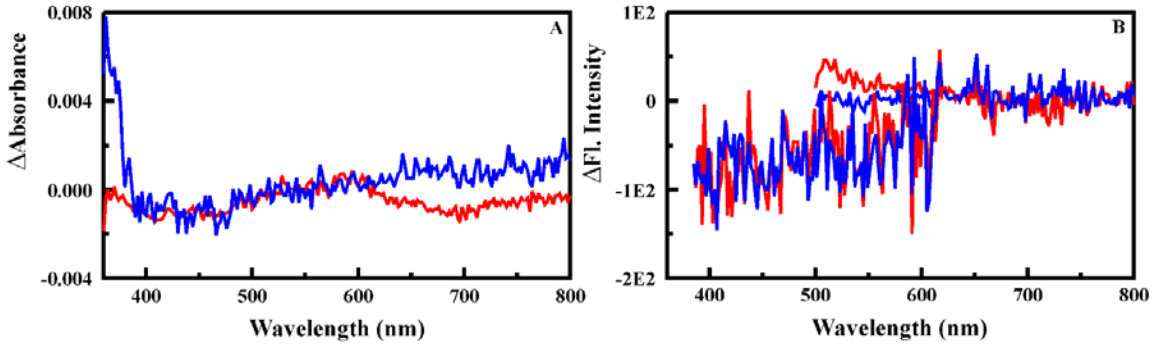

Figure A6. C_1-Indol binding isotherms. Full data sets for the interaction of C_1-Indol with *E. coli* and *B. cereus* at varied cell and tracer concentrations. (A) Absorbance changes for *E. coli* interaction, 432 nm. (B) Fluorescence change for *E. coli* interaction, 650 nm. (C) Absorbance change for *B. cereus* interaction, 432 nm. (D) Fluorescence change for *B. cereus* interaction, 650 nm. Lines indicate the fit contour generated for the cell concentration of the matching color. Fit parameters provided in Table 2.

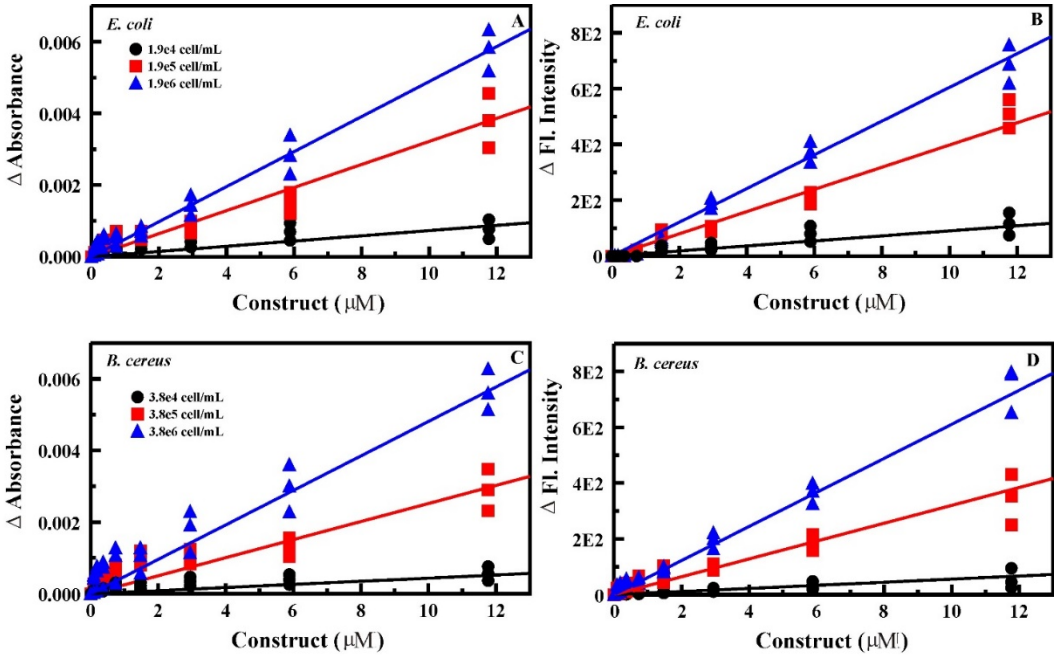

Figure A7. C_1-CeMe binding isotherms. Full data sets for the interaction of C_1-CeMe with *E. coli* and *B. cereus* at varied cell and tracer concentrations. (A) Absorbance changes for *E. coli* interaction, 427 nm. (B) Fluorescence change for *E. coli* interaction, 658 nm. (C) Absorbance change for *B. cereus* interaction, 427 nm. (D) Fluorescence change for *B. cereus* interaction, 658 nm. Lines indicate the fit contour generated for the cell concentration of the matching color. Where full contours are not included (green circles), x marks the calculated value from the fit. Fit parameters provided in Table 2.

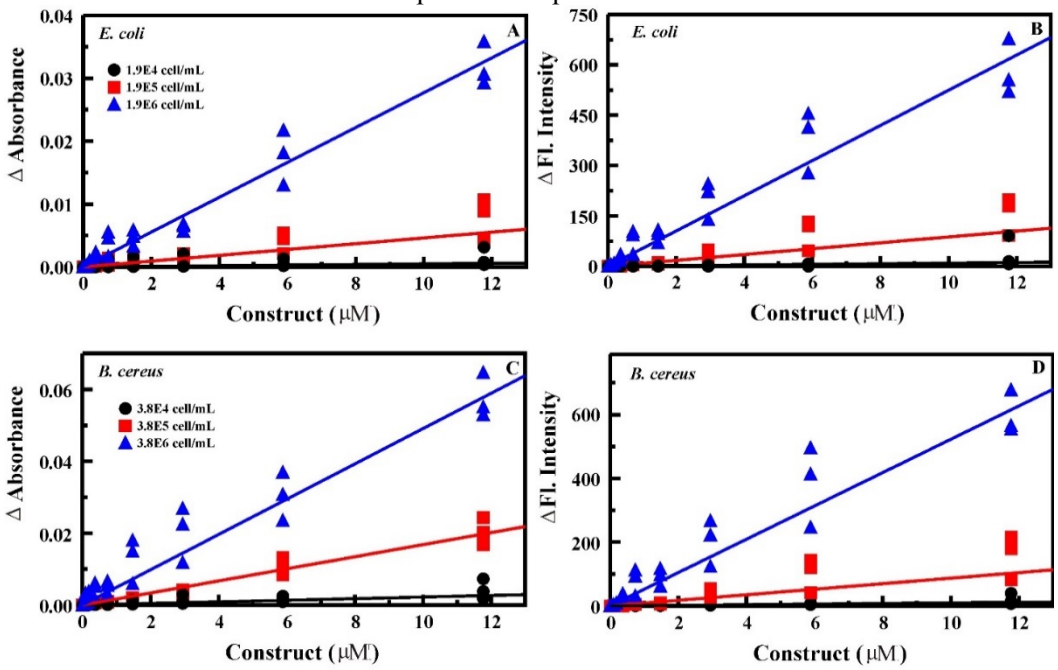

APPENDIX B

ADDITIONAL DATA & ANALYSIS FOR METAL C_1TPP CONSTRUCTS

Figure B1. Metal C_1-CeMe constructs. Absorbance and fluorescence spectra for the C_1-CeMe variants (7.8 μM). The spectrophotometric characteristics for the C_1TPP-cercropin A-melittin hybrid construct are presented for the vanadium (blue), cobalt (red), and zinc (green) complexes as well as the original construct (black).

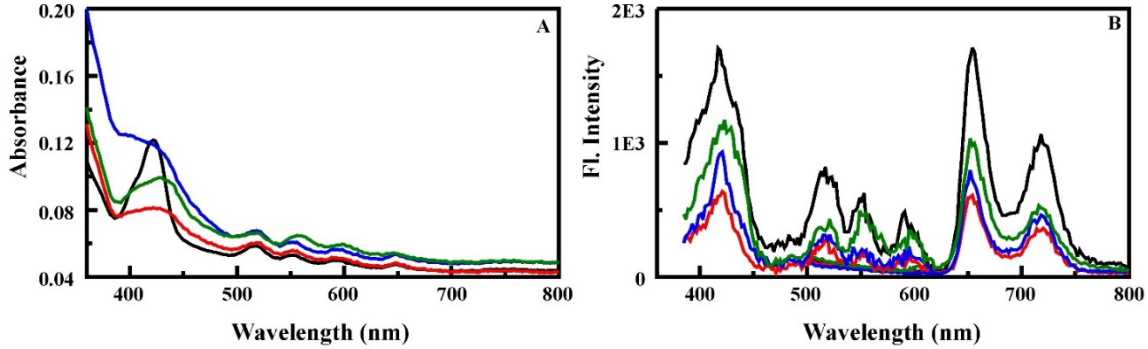

Figure B2. Metal C_1-Bac constructs. Absorbance and fluorescence spectra for the C_1-Bac variants (7.8 μM). The spectrophotometric characteristics for the C_1TPP-bactenecin construct are presented for the vanadium (blue), cobalt (red), and zinc (green) complexes as well as the original construct (black).

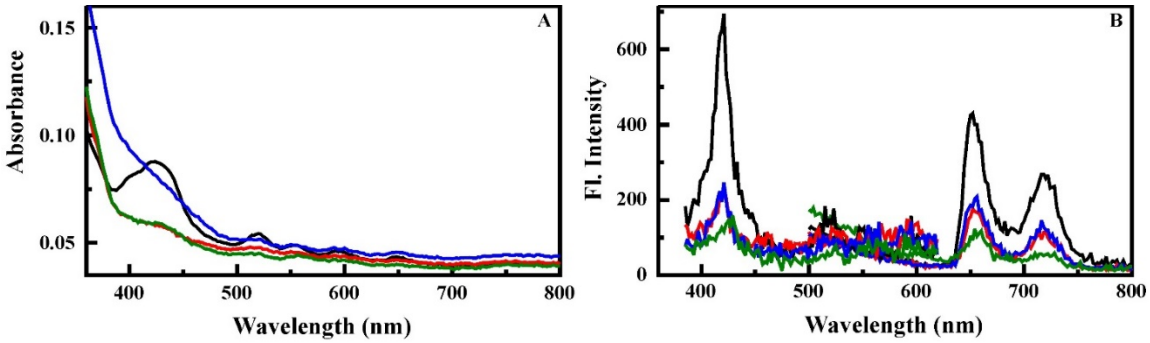

Figure B3. Metal C_1-PME constructs. Absorbance and fluorescence spectra for the C_1-PME variants (7.8 μM). The spectrophotometric characteristics for the C_1TPP-PME construct are presented for the vanadium (blue), cobalt (red), and zinc (green) complexes as well as the original construct (black).

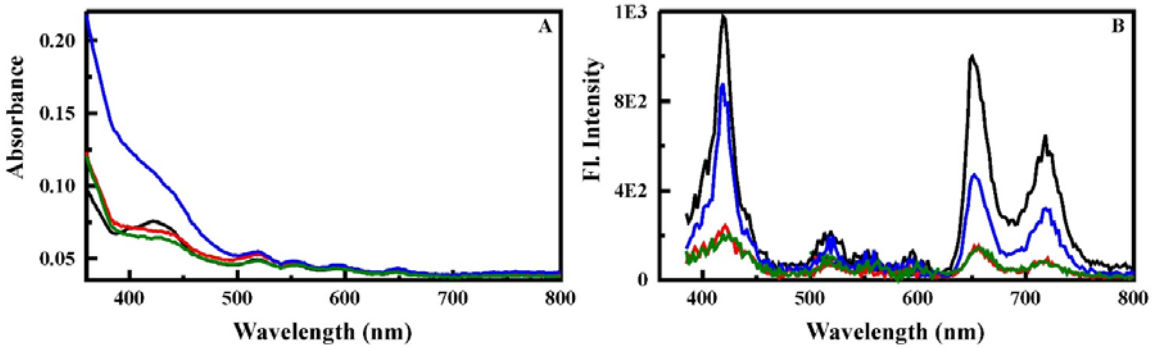

Figure B4. Metal C_1-Indol constructs. Absorbance and fluorescence difference spectra for the interaction of ZnC_1-Indol (A and B), VC_1-Indol (C and D), and CoC_1-Indol (E and F) (all at 12 μM) with *E. coli* (red; 1.9×10^6 cell/mL) and *B. cereus* (blue; 2.0×10^6 cell/mL).

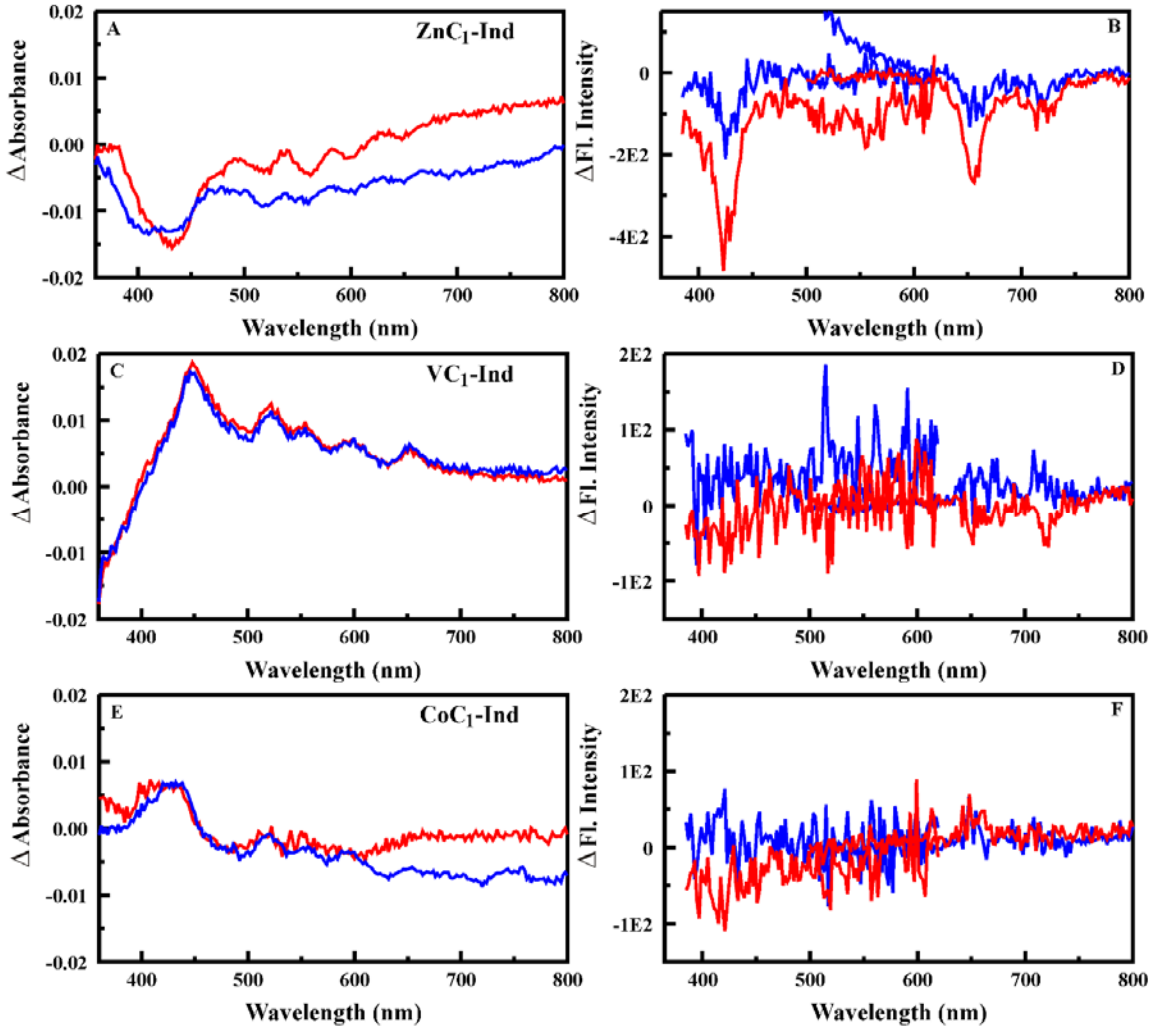

Figure B5. Metal C_1-CeMe constructs. Absorbance and fluorescence difference spectra for the interaction of ZnC_1-CeMe (A and B), VC_1-CeMe (C and D), and CoC_1-CeMe (E and F) (all at 12 μM) with *E. coli* (red; 1.9×10^6 cell/mL) and *B. cereus* (blue; 2.0×10^6 cell/mL).

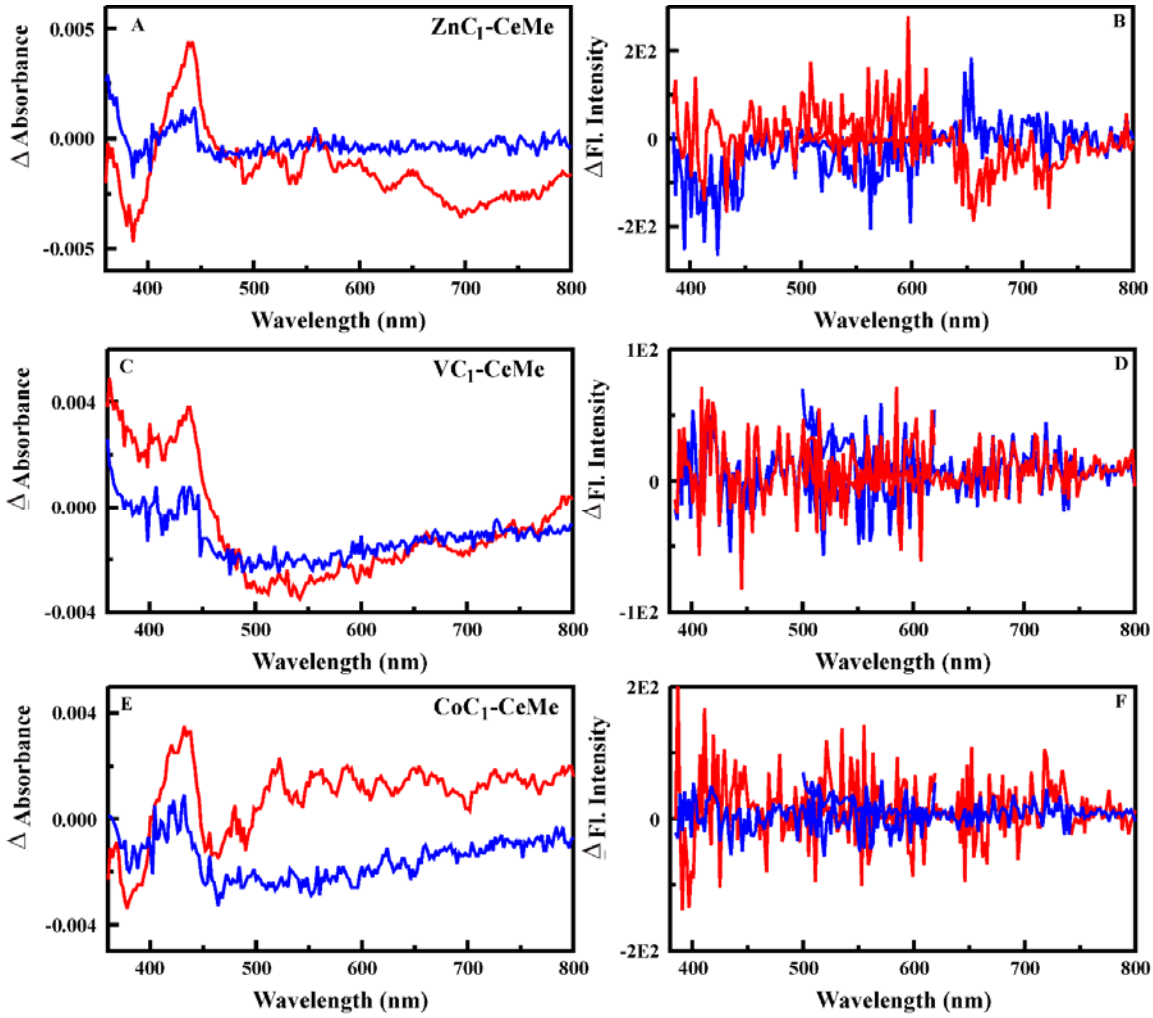

Figure B6. Metal C_1-Bac constructs. Absorbance and fluorescence difference spectra for the interaction of ZnC_1-Bac (green), VC_1-Bac (blue), and CoC_1-Bac (red) (all at 12 μM) with *E. coli* (A and B; 1.9×10^6 cell/mL) and *B. cereus* (C and D; 2.0×10^6 cell/mL).

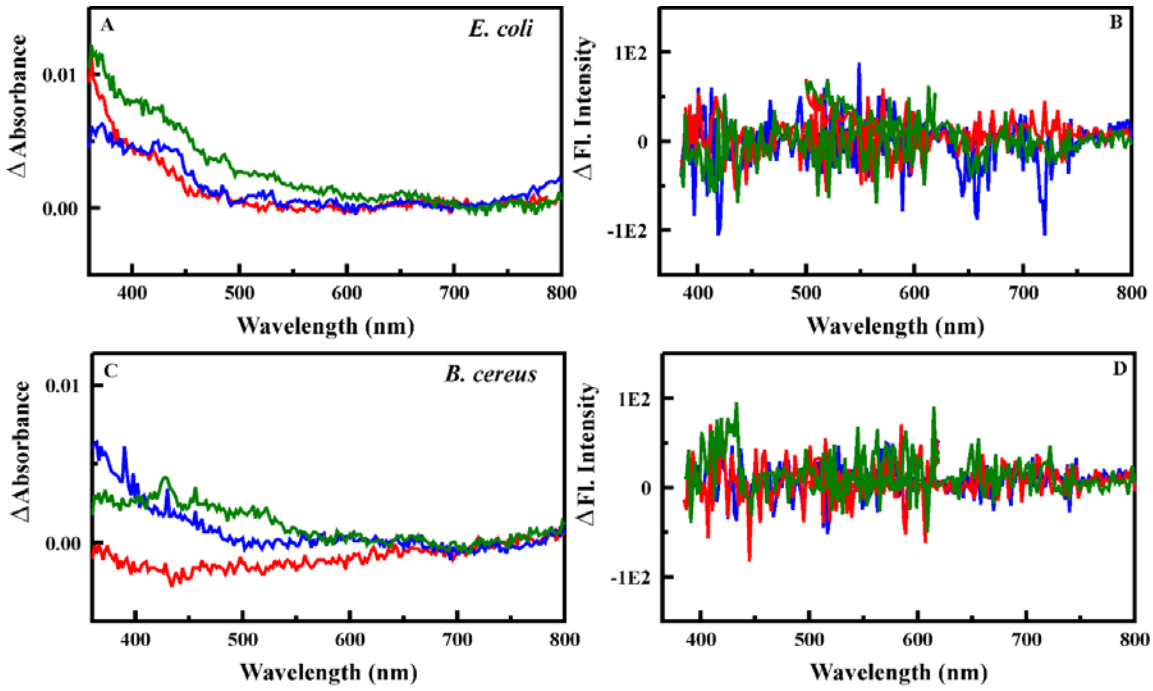

Figure B7. Metal C_1-PME constructs. Absorbance and fluorescence difference spectra for the interaction of ZnC_1-PME (green), VC_1-PME (blue), and CoC_1-PME (red) (all at 12 μM) with *E. coli* (A and B; 1.9×10^6 cell/mL) and *B. cereus* (C and D; 2.0×10^6 cell/mL).

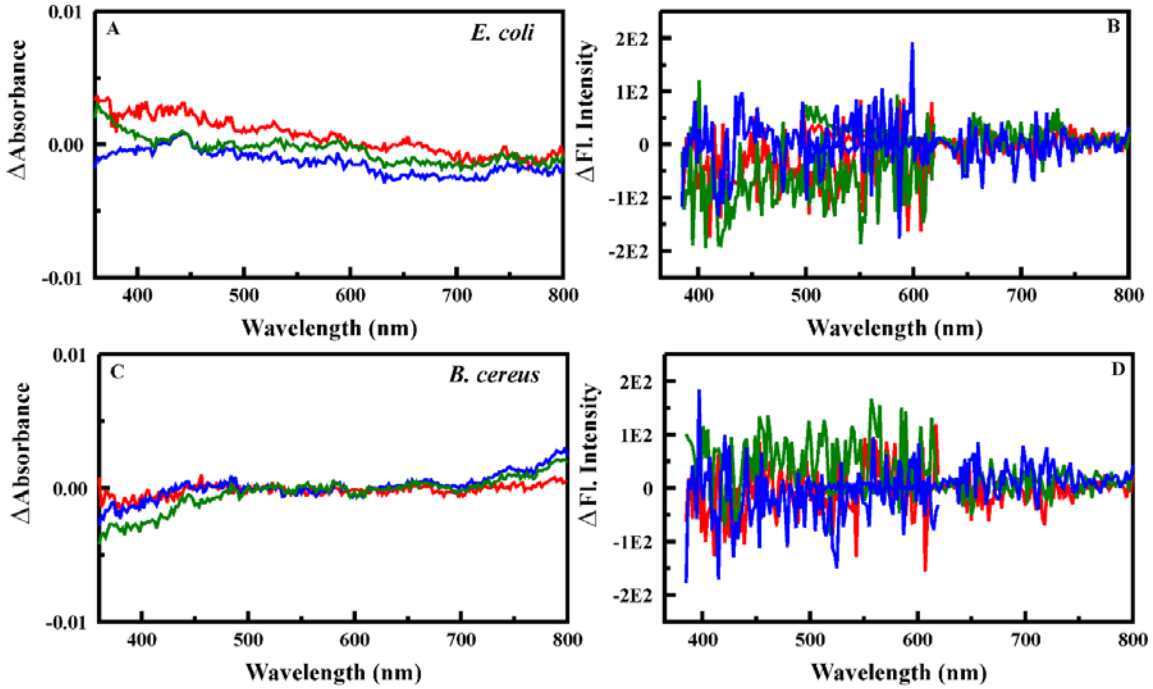

Figure B8. Metal C_1-Indol binding isotherms. Full data sets for the interaction of the metal C_1-Indol variants with *E. coli* and *B. cereus* at varied cell and tracer concentrations. (A) Absorbance changes for interaction of ZnC1-Indol with *E. coli*, 428 nm. (B) Fluorescence changes for interaction of ZnC1-Indol with *E. coli*, 650 nm. (C) Absorbance changes for interaction of ZnC1-Indol with *B. cereus*, 428 nm. (D) Fluorescence changes for interaction of ZnC1-Indol with *B. cereus*, 650 nm. (E) Absorbance changes for interaction of CoC1-Indol with *E. coli*, 422 nm. (F) Absorbance changes for interaction of CoC1-Indol with *B. cereus*, 422 nm. (G) Absorbance changes for interaction of VC1-Indol with *E. coli*, 446 nm. (H) Absorbance changes for interaction of VC1-Indol with *B. cereus*, 446 nm. Lines indicate the fit contour generated for the cell concentration of the matching color. Fit parameters provided in Table 2.

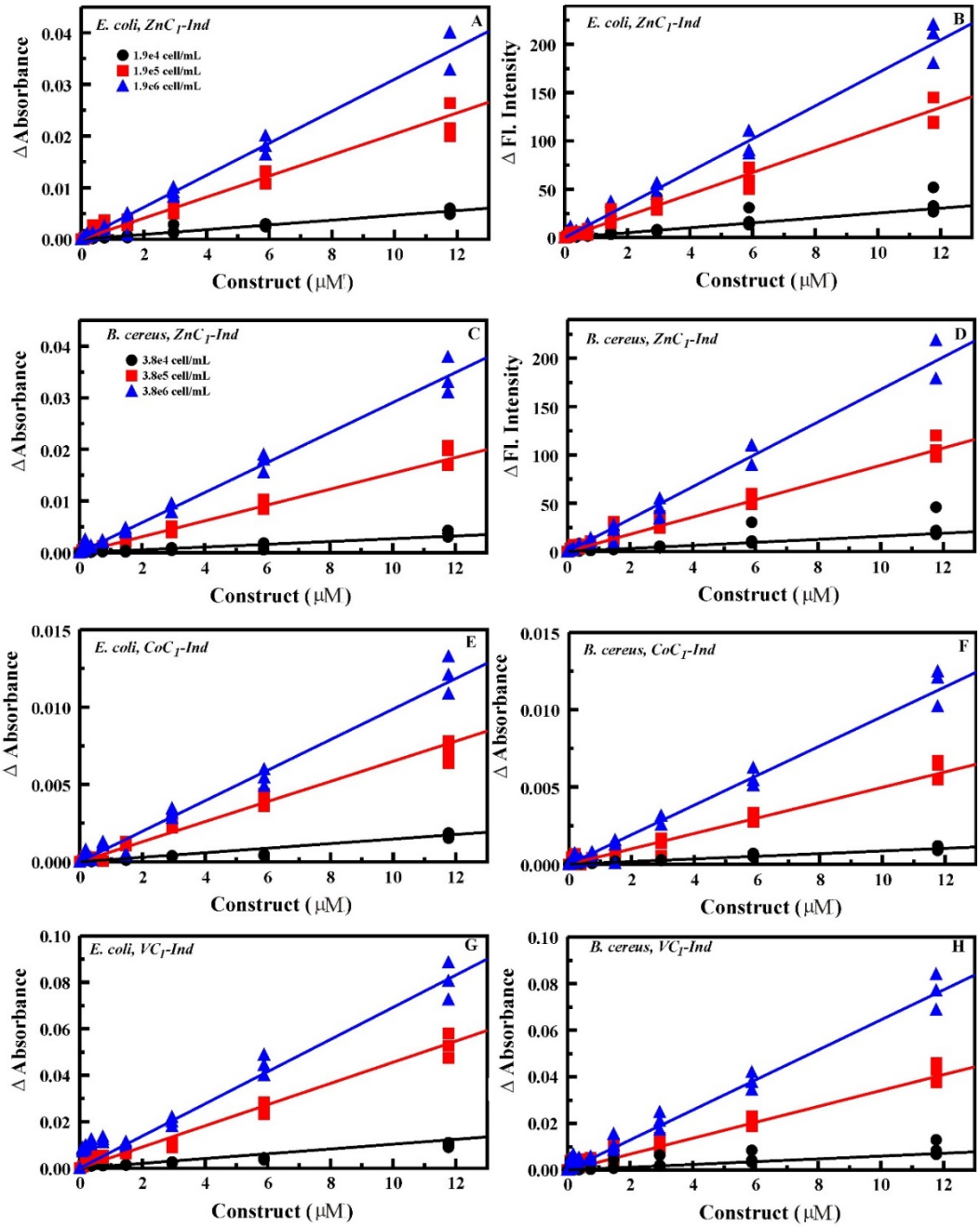

Figure B9. Metal C_1-CeMe binding isotherms. Full data sets for the interaction of the metal C_1-CeMe variants with *E. coli* at varied cell and tracer concentrations. (A) Absorbance changes for interaction of CoC1-CeMe with *E. coli*, 427 nm. (B) Absorbance changes for interaction of VC1-CeMe with *E. coli*, 435 nm. (C) Absorbance changes for interaction of ZnC1-CeMe with *E. coli*, 440 nm. (D) Fluorescence changes for interaction of ZnC1-CeMe with *E. coli*, 660 nm. Lines indicate the fit contour generated for the cell concentration of the matching color. Fit parameters provided in Table 2.

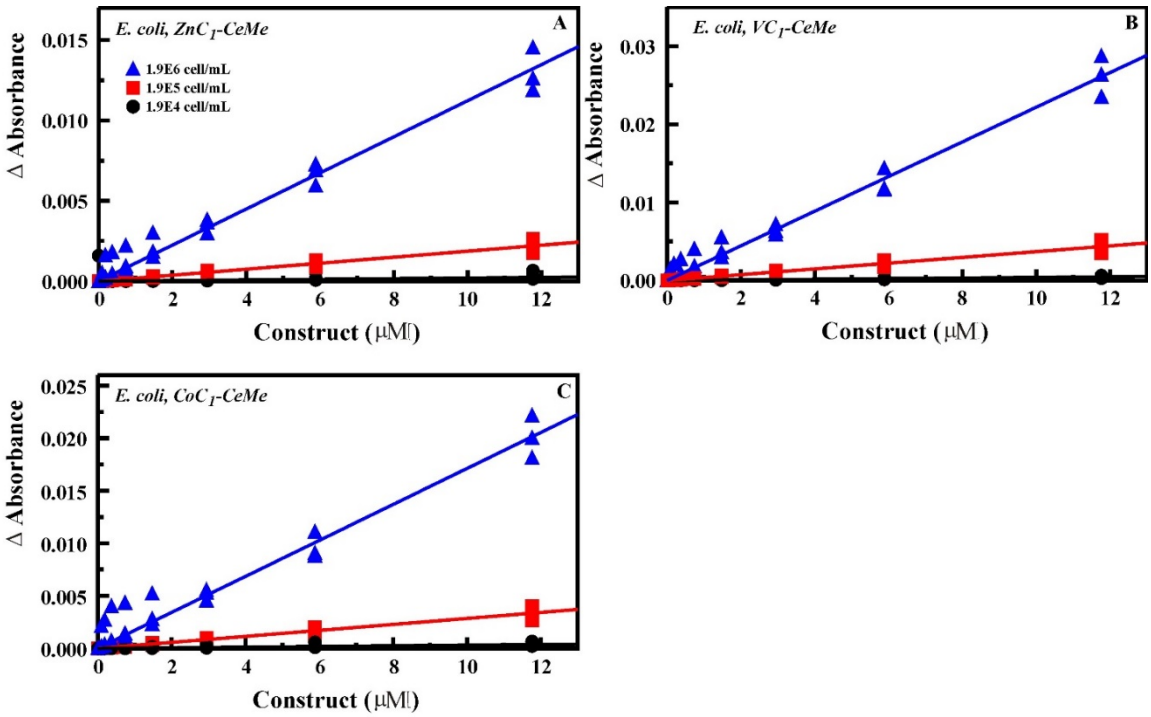

APPENDIX C

ADDITIONAL DATA & ANALYSIS FOR CEME(S)-C_1TPP CONSTRUCT

Figure C1. The C_1-CeMe(S) indicator. Absorbance (left) and fluorescence (right) spectra for the C_1-CeMe(S) construct (concentrations in μM provided in the legend). Below, the peak intensity versus concentration is provided. All compounds in 15% DMSO.

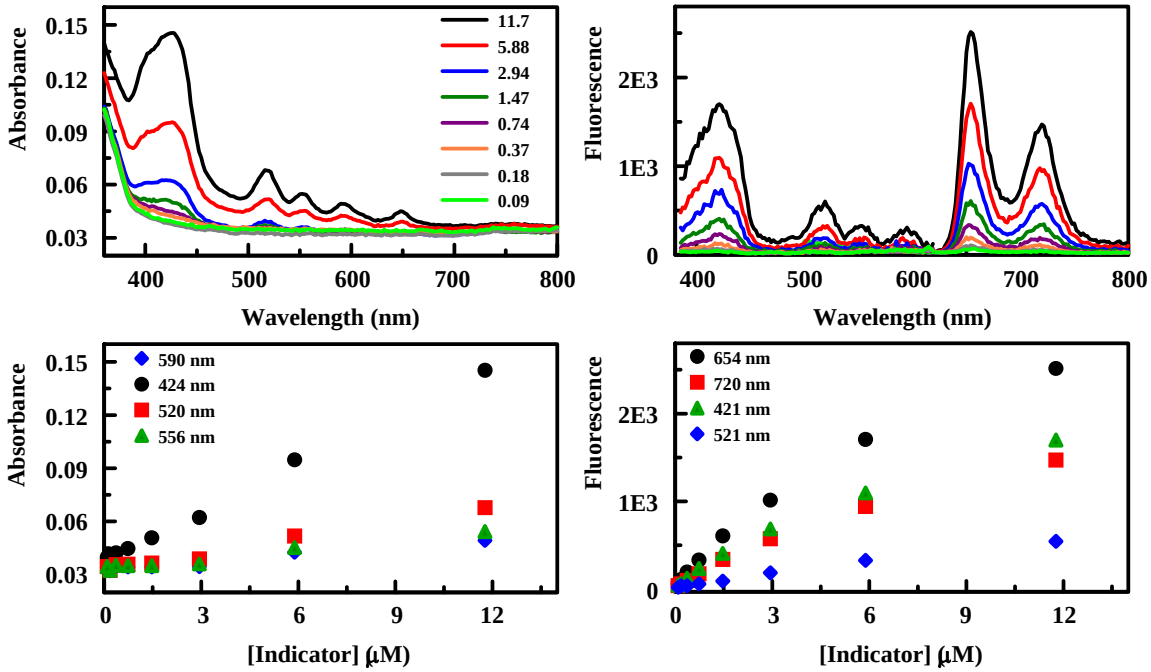

Figure C2. Interaction of C_1-CeMe(S) with *E. coli*. Absorbance (left) and fluorescence (right) spectra for C_1-CeMe(S) (11.8 μM) in the presence and absence (black) of bacterial cells (concentrations in cells/mL provided in the legend). All solutions contain 15% DMSO.

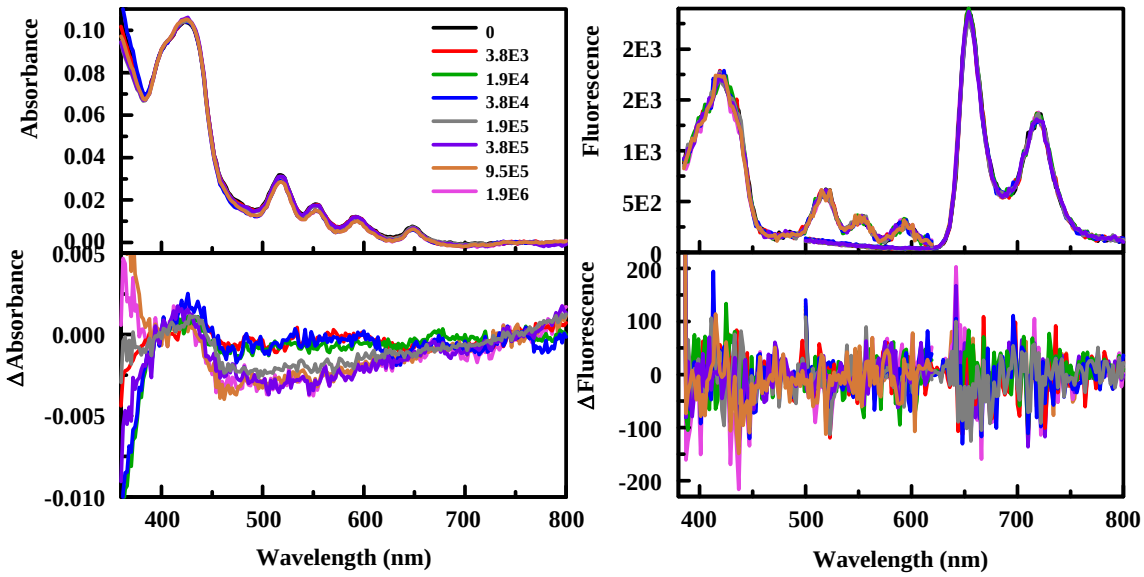

Figure C3. Interaction of C_1-CeMe(S) with *B. cereus*. Absorbance (left) and fluorescence (right) spectra for C_1-CeMe(S) (11.8 μM) in the presence and absence (black) of bacterial cells (concentrations in cells/mL provided in the legend). All solutions contain 15% DMSO.

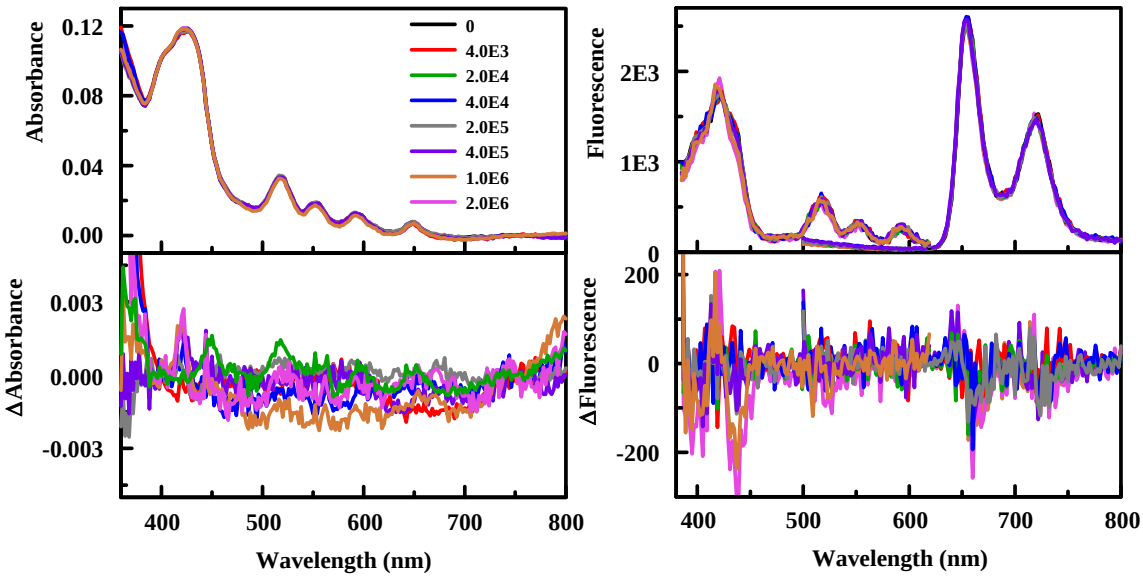

APPENDIX D

ADDITIONAL DATA & ANALYSIS FOR C_1S_3TPP CONSTRUCTS

Figure D1. The C_1S_3-Indol indicator. Absorbance (left) and fluorescence (right) spectra for the C_1S_3-Indol construct (concentrations in μM provided in the legend). Below, the peak intensity versus concentration is provided. All compounds in 15% DMSO.

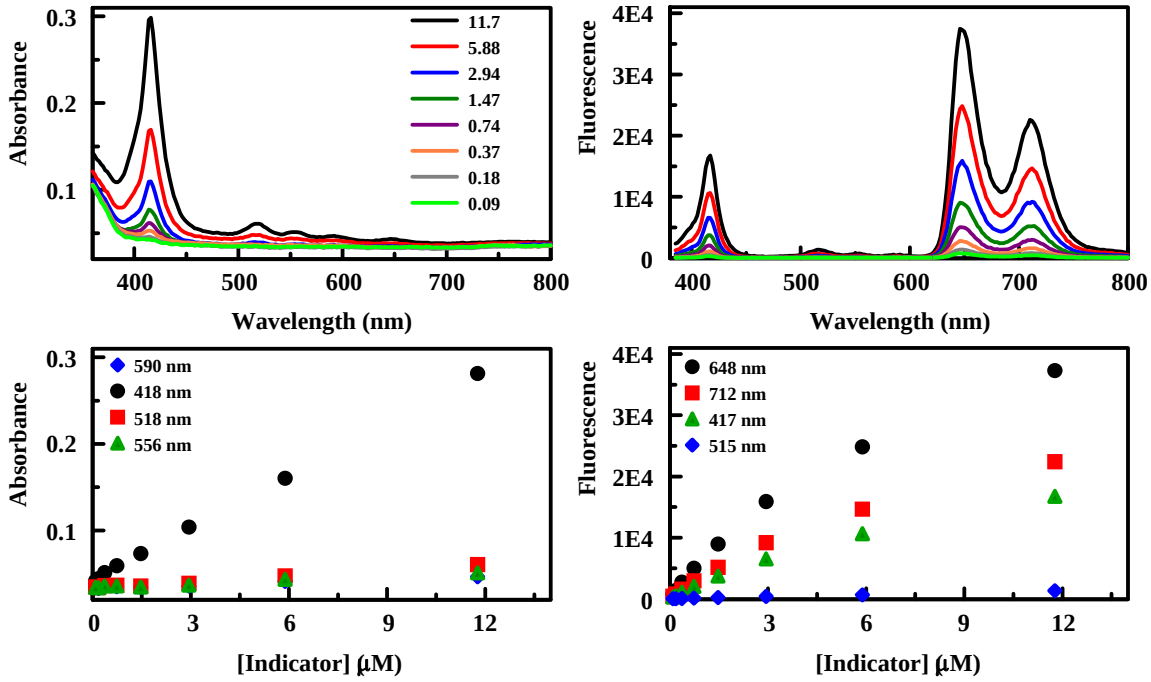

Figure D2. Interaction of C_1S_3-Indol with *E. coli*. Absorbance (left) and fluorescence (right) spectra for C_1S_3-Indol (11.8 μM) in the presence and absence (black) of bacterial cells (concentrations in cells/mL provided in the legend). All solutions contain 15% DMSO.

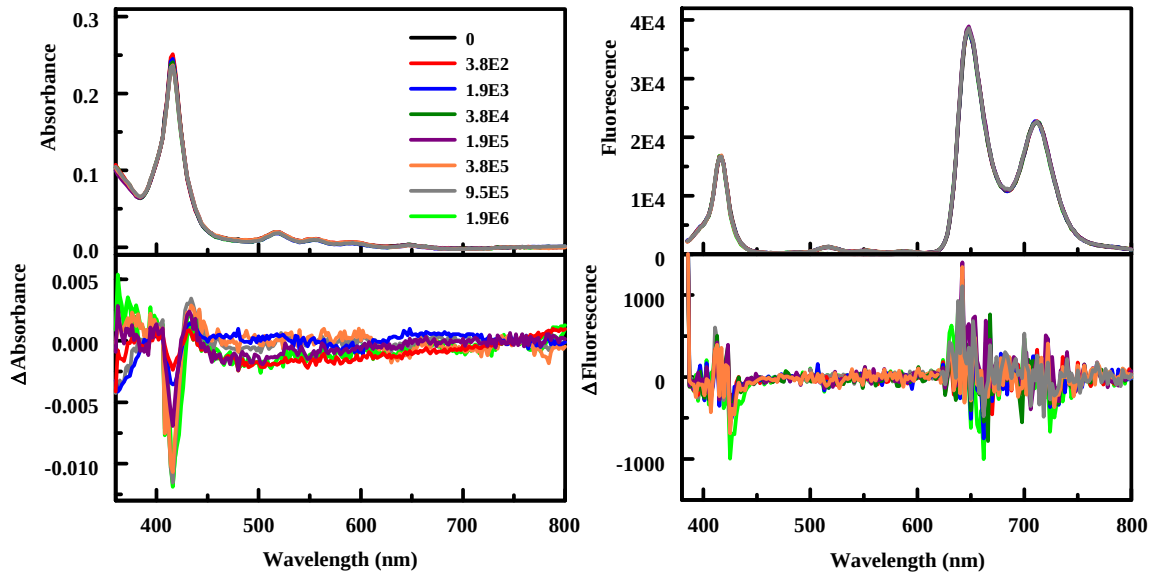

Figure D3. Interaction of C_1S_3-Indol with *B. cereus*. Absorbance (left) and fluorescence (right) spectra for C_1S_3-Indol (11.8 μM) in the presence and absence (black) of bacterial cells (concentrations in cells/mL provided in the legend). All solutions contain 15% DMSO.

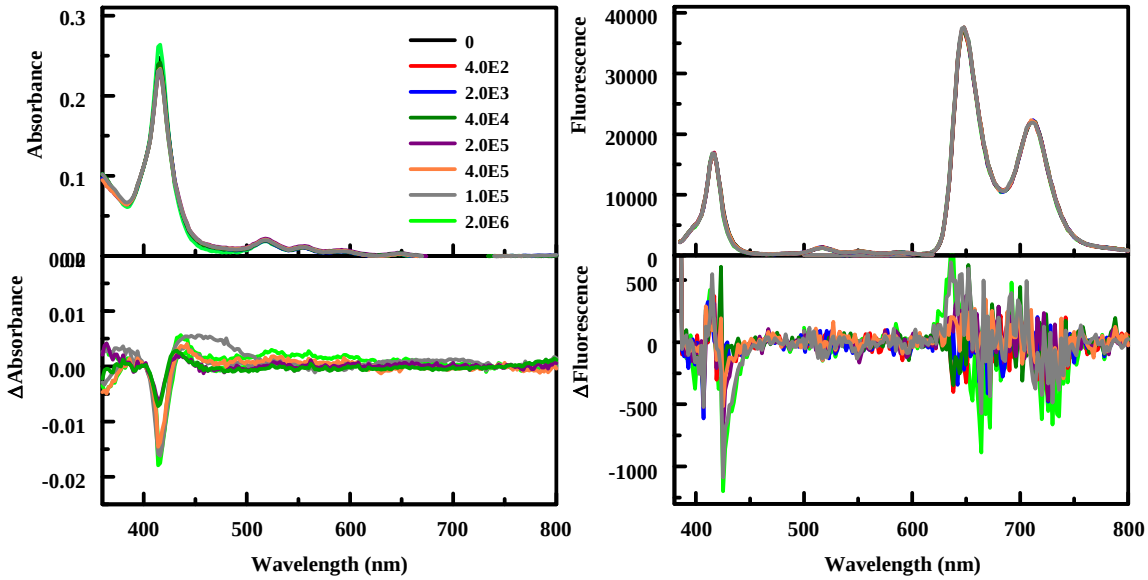

Figure D4. The C_1S_3-CeMe(S) indicator. Absorbance (left) and fluorescence (right) spectra for the C_1S_3-CeMe(S) construct (concentrations in μM provided in the legend). Below, the peak intensity versus concentration is provided. All compounds in 15% DMSO.

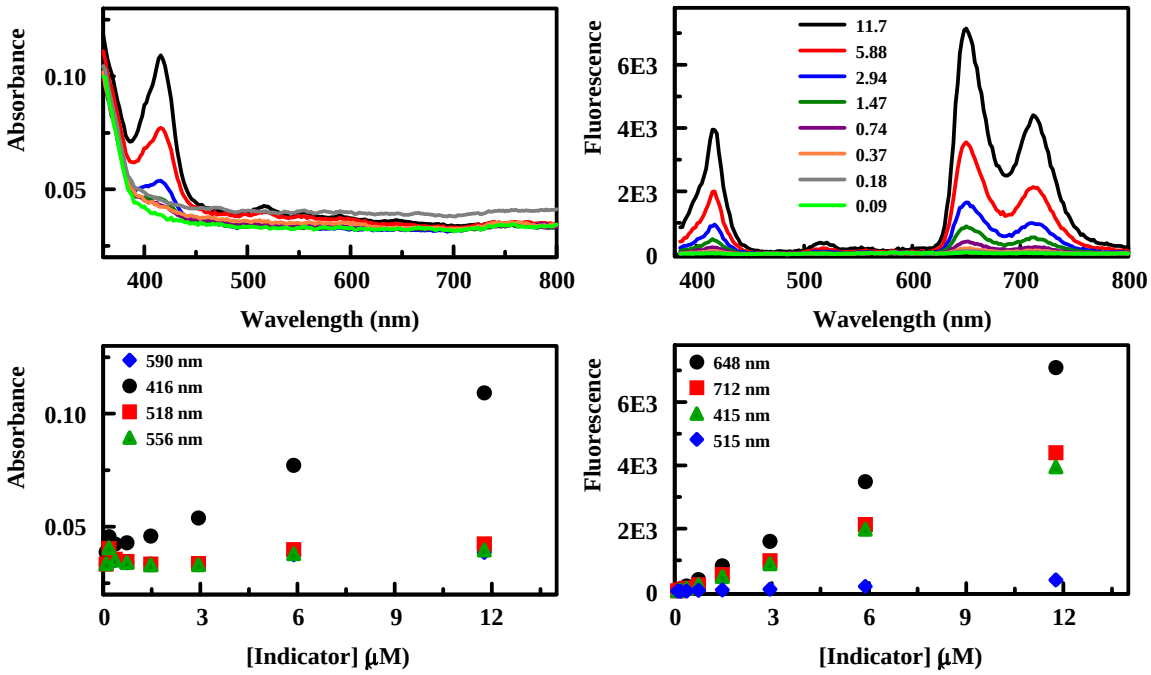

Figure D5. Interaction of C_1S_3-CeMe(S) with *E. coli*. Absorbance (left) and fluorescence (right) spectra for C_1S_3-CeMe(S) (11.8 μM) in the presence and absence (black) of bacterial cells (concentrations in cells/mL provided in the legend). All solutions contain 15% DMSO.

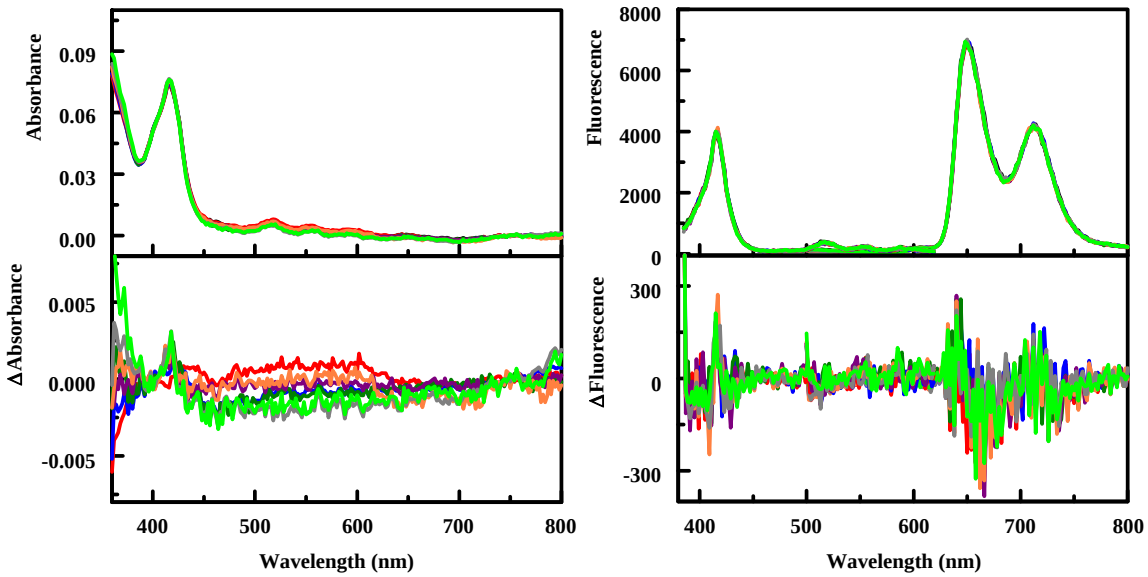

Figure D6. Interaction of C_1S_3-CeMe(S) with *B. cereus*. Absorbance (left) and fluorescence (right) spectra for C_1S_3-CeMe(S) (11.8 μM) in the presence and absence (black) of bacterial cells (concentrations in cells/mL provided in the legend). All solutions contain 15% DMSO.

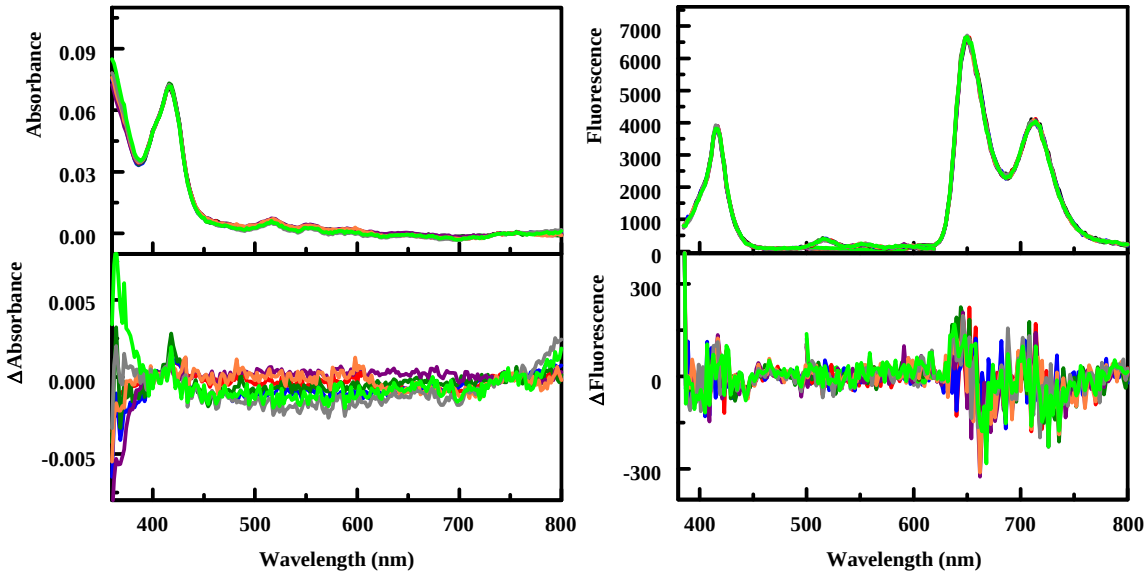

Figure D7. The C_1S_3-CeMe(L) indicator. Absorbance (left) and fluorescence (right) spectra for the C_1S_3-CeMe(L) construct (concentrations in μM provided in the legend). Below, the peak intensity versus concentration is provided. All solutions include 15% DMSO.

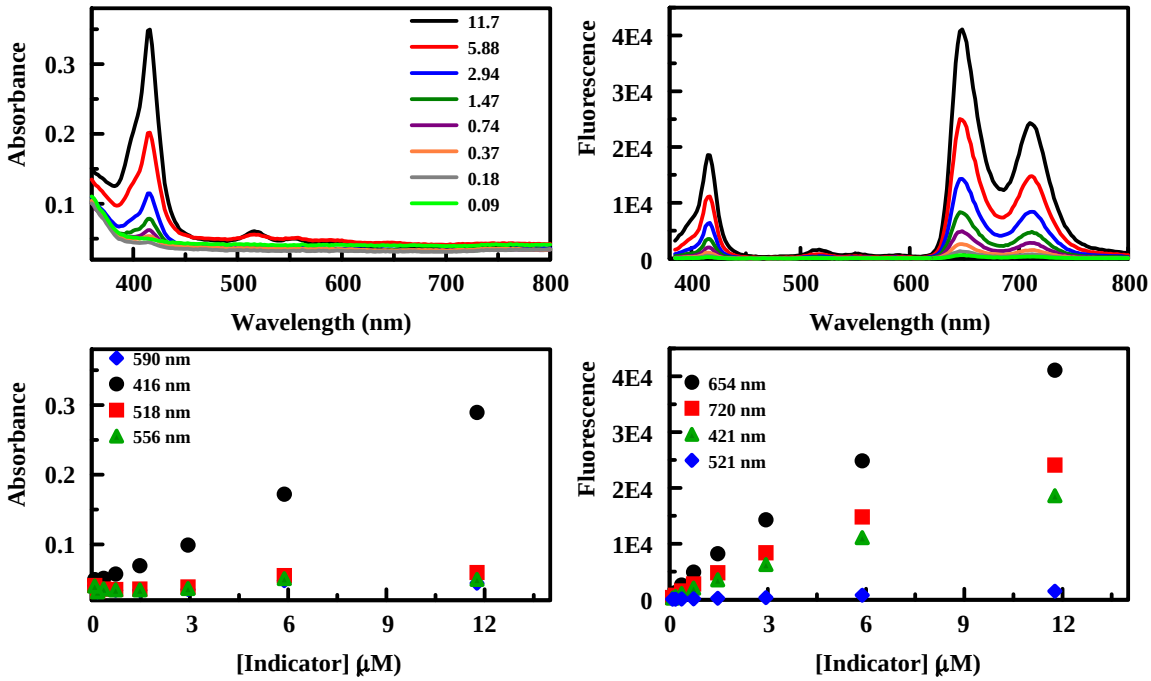

Figure D8. Interaction of C_1S_3-CeMe(L) with *E. coli*. Absorbance (left) and fluorescence (right) spectra for C_1S_3-CeMe(L) (11.8 μM) in the presence and absence (black) of bacterial cells (concentrations in cfu/mL provided in the legend). All solutions contain 15% DMSO.

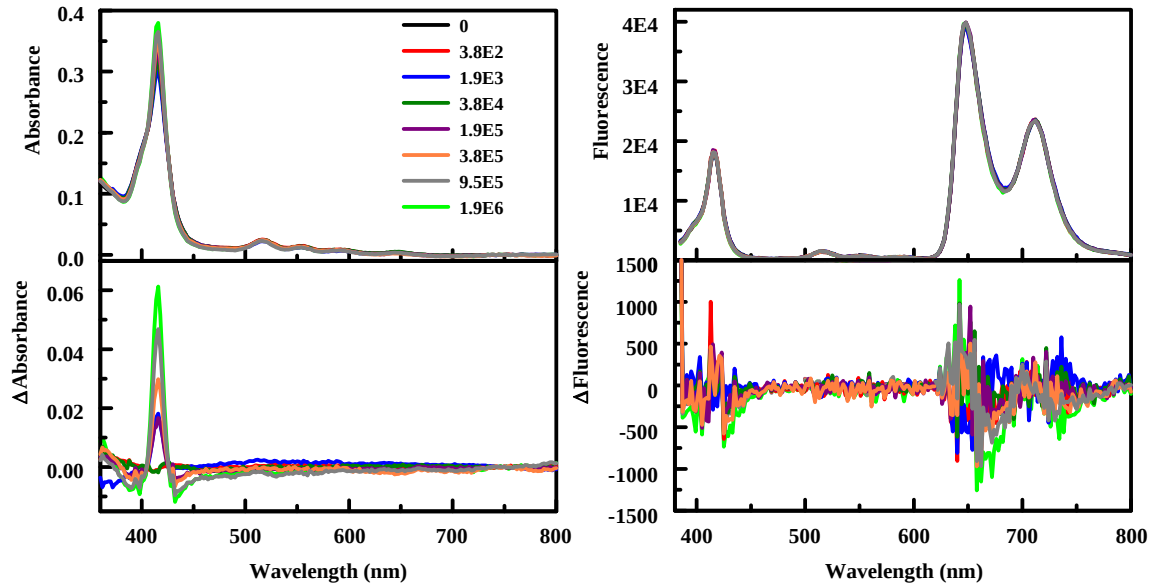

Figure D9. Interaction of C_1S_3-CeMe(L) with *B. cereus*. Absorbance (left) and fluorescence (right) spectra for C_1S_3-CeMe(L) (11.8 μM) in the presence and absence (black) of bacterial cells (concentrations in cfu/mL provided in the legend). All solutions contain 15% DMSO.